



HAL
open science

Dynamic crushing of wood-based sandwich composite tubes

Romain Guélou, Florent Eyma, Arthur Cantarel, Samuel Rivallant, Bruno Castanié

► **To cite this version:**

Romain Guélou, Florent Eyma, Arthur Cantarel, Samuel Rivallant, Bruno Castanié. Dynamic crushing of wood-based sandwich composite tubes. *Mechanics of Advanced Materials and Structures*, 2021, pp.1-21. 10.1080/15376494.2021.1991533 . hal-03407710

HAL Id: hal-03407710

<https://hal.science/hal-03407710>

Submitted on 28 Oct 2021

HAL is a multi-disciplinary open access archive for the deposit and dissemination of scientific research documents, whether they are published or not. The documents may come from teaching and research institutions in France or abroad, or from public or private research centers.

L'archive ouverte pluridisciplinaire **HAL**, est destinée au dépôt et à la diffusion de documents scientifiques de niveau recherche, publiés ou non, émanant des établissements d'enseignement et de recherche français ou étrangers, des laboratoires publics ou privés.

Dynamic crushing of wood based sandwich composite tubes

R. Guélou^a, F. Eyma^a, A. Cantarel^a, S. Rivallant^a, B. Castanié^{a,*}

^aInstitut Clément Ader (ICA), ISAE, CNRS UMR 5312-INSA-Mines Albi-UPS, Toulouse, France

* Corresponding author: bruno.castanie@insa-toulouse.fr

Keywords: Wood veneers, Poplar, Composites, Sandwich, Crushing, Energy absorption, Tube, Dynamic

Abstract: The paper presents the results of dynamic crushing of sandwich tubes that had skins made of carbon or glass fibres - with epoxy resin - and an I214 poplar ply core. By increasing the number of poplar plies from two to six, the absorbed energy is doubled, showing the significant contribution of the wood. The Specific Energy Absorption of sandwiches with carbon fibre skins oscillated between 49.4 and 60 J/g while that with glass fibre skins varied from 35.4 to 43.3 J/g.

1. Introduction

Wood is a material that is respectful of the environment because it is renewable and requires little embodied energy (energy corresponding to the transformation of the raw product into the finished product) due to its ability to store carbon [1,2]. Wood is considered to be a credible substitute material for meeting sustainable development targets, particularly in the field of transport [3]. It is a material that has been used for many years in both civil engineering and aeronautics, where planes were made of wood until World War II and showed remarkable levels of performance [4]. Several French companies are showing renewed interest by either pursuing wood construction (Robin Aircraft [5]) with the DR401 (2700 units since 1972) or introducing it into their most recent structures ([6,7]). Studies have also shown that this material is particularly interesting for automobiles [8,9]. This renewal of interest is also shared by the academic world and recent studies demonstrate the interest of wood alone or in combination with natural fibres or modern materials such as glass, Kevlar, carbon or even aluminium, in particular in sandwich form [10-16]. An increasing number of recent academic studies have also shown

28 that wood has very good mechanical characteristics at low speed-low energy impact [17-23] and in
29 compression after impact, with behaviour that is sometimes surprising compared to that of composites.
30 The knockdown factor can reach 70 % for classical carbon Nomex sandwich and is less than 10% in
31 certain configurations with plywood cores [24-26]. Historically, wood has also been identified as a
32 material with good dynamic and crash absorption characteristics and has been used for a very long
33 time, for example, in the transport of radioactive materials [27–28].

34 In previous papers, the authors looked into the crash behaviour of tubes laminated with plies in poplar
35 alone I214 [29] and were able to show that this wood, one of the cheapest and lightest, had good SEA
36 up to 30 J / kg for a material 40 times less expensive than CFRP, and renewable. As with composite
37 tubes, exterior polar plies oriented at 90° and creating a “hoop effect” increased resistance to the
38 crushing force, thus improving the SEA. It is therefore clear that sandwich tubes with a core in I214
39 poplar plies and the interior and exterior skins of the tube in carbon and fibreglass fabrics should be the
40 next step. These configurations have been tested under quasi-static loads in [30].

41 It was shown that better energy absorption was obtained with all the poplar veneers at 0° because the
42 “hoop effect” ensured by the outer and inner composite layers was sufficient. The average SEA of tubes
43 with carbon skins was 61.2 J/g and remains quite constant, for an SEA gain of around 47% with respect
44 to the sum of the two materials crushed independently. An average SEA of 32.5 J/g was obtained for
45 tubes with glass skins. Coupling I214 poplar veneers with glass fibres allowed, in particular, a gain of
46 20% on absorbed energy and 22% on the SEA.

47 This paper is the continuation of [30] and presents the dynamic crushing of sandwich tubes with
48 composite skins in carbon or glass fibres and a core in I214 poplar veneers. The objective is to
49 understand the behaviour of these structures from the point of view of dynamics.

50

51 **2. Materials, test specimens and setup**

52 **2.1. Materials and manufacturing**

53 The sandwich tubes were manufactured using a metal mandrel, on which the two inner composite
54 layers (carbon or glass fabrics) were stacked first. It was presented in [30] and is briefly recalled here.
55 The 1 mm thick I214 poplar veneers, supplied by the Garnica company, were then wound up. A heat-
56 shrinkable tape was wound around them to provide pressure during crosslinking. After this first curing
57 cycle, the 2 outer composite plies (carbon or glass fabrics) were finally stacked and a second curing
58 cycle was performed with a wound heat-shrink band.

59 The monolithic carbon or glass tubes were manufactured in the same way: four composite plies were
60 stacked over the metal mandrel and a heat-shrinkable strip was wound around them. The curing cycles
61 were as follows:

62 - For carbon, 30 min at 90 °C then 2 h 20 min at 120 °C,

63 - For glass, 30 min at 90 °C then 1 hour at 120 °C.

64 The prepregs used were supplied by Hexcel: the carbon plies were made with the prepreg
65 M79/42%/200T2/ CHR-3K and the glass plies were in prepreg M9.6GF/42%/200T2/G, inducing
66 theoretical fibre volume fractions of 44% and 39% respectively. These two prepregs were 2-2 twills
67 having an areal weight of 345 g/m² and were oriented at [0/90] to obtain a hoop effect.

68 The wood glue used to pre-glue the veneers before they were rolled up was Kleiberit PUR 510
69 FIBERBOND glue, a one-component polyurethane-based glue that hardens by reaction with humidity,
70 with a basis weight of 250 g/m². When the I214 poplar veneers had been stacked around the mandrel,
71 the bonding was carried out with a relative humidity of between 8.8 and 9.8%. The density of the I214
72 veneers was 0.368 g/cm³.

73 The inner diameter of the tubes was 50 mm and their final length was 120 mm. A 45° chamfer was
74 made around the entire thickness of the tubes (Fig. 1) in order to lower the peak load and control the
75 side of failure initiation.

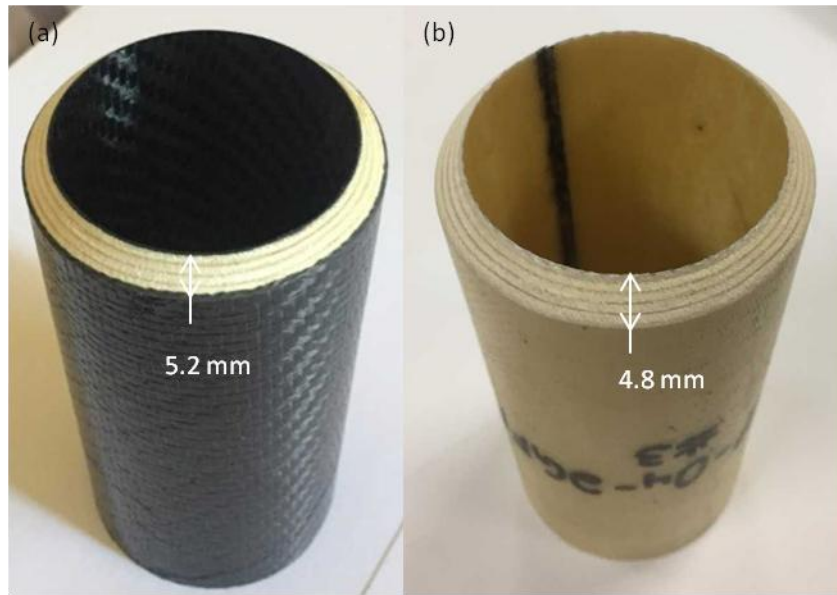


Fig. 1: Pristine sandwich tubes, (a) [2CFRP-[0₄]-2CFRP]-#3, (b) [2CFRP-[0₄]-2CFRP]-#3

76

77

78 The effect of wood was studied by varying the number of I214 plies from two to six while keeping a
 79 constant number of interior and exterior composite plies (carbon or glass). A sandwich tube had two
 80 interior composite plies and two exterior plies that thus constituted the skins. The composite tubes
 81 alone, intended for the evaluation of the coupling effects, then had four 4 plies in total. The sandwich
 82 tubes were defined by the following notation: [2GFRP- [0_n]-2GFRP] describing two glass plies on the
 83 inside and two plies on the outside, and n poplar plies oriented at 0° (0° being the longitudinal axis of
 84 the tube). The composite tubes were then defined by the notation [GFRP] or [CFRP] depending on the
 85 nature of the fibres. They always had four plies in total.

| | Dynamic | | Dynamic |
|---|---------|---------------------------------|---------|
| [2CFRP-[0 ₆]-2CFRP] | 3 | [2GFRP-[0 ₆]-2GFRP] | 3 |
| [2CFRP-[0 ₅]-2CFRP] | 3 | [2GFRP-[0 ₅]-2GFRP] | 3 |
| [2CFRP-[0 ₄]-2CFRP] | 3 | [2GFRP-[0 ₄]-2GFRP] | 3 |
| [2CFRP-[0 ₃]-2CFRP] | 3 | [2GFRP-[0 ₃]-2GFRP] | 3 |
| [2CFRP-[0 ₂]-2CFRP] | 3 | [2GFRP-[0 ₂]-2GFRP] | 3 |
| [CFRP] | 3 | [GFRP] | 3 |
| [90/0 ₄ /90] (already crushed in [29]) | 3 | | |
| Total number of tubes | | 39 | |

Tab. 1: Summary of the test matrix

86

87 The poplar veneers were characterized mechanically in [30] by carrying out six tensile tests on a
88 specimen of two l214 plies glued together in the transverse and longitudinal directions (same wood glue
89 and same areal density).

90 **2.2. Dynamic setup**

91 As in [29], the dynamic tests were performed using a drop weight tower (Fig. 2). The initial crushing
92 speeds were between 8.4 and 8.8 m / s. The device was equipped with a ballast mass (81 or 114 kg
93 depending on the number of poplar plies). The mass of ballast was sufficient to provide more energy
94 than that absorbed by the tube, so as to obtain an almost constant crushing speed. The excess energy
95 was collected by a stop system that transferred this excess to honeycombs located below the lower
96 plate. The stops allowed approximately 85-90 mm to be crushed and enabled observation of the tubes
97 after crushing. A 100 kN force sensor was located between the (upper) crushing plate and the masses
98 so that the force during the crushing could be acquired at a frequency of 1 MHz. A method of double
99 integration from the effort and the initial speed gave the displacement. The movement was also verified
100 by means of images from high speed cameras that were synchronized with the force sensor.

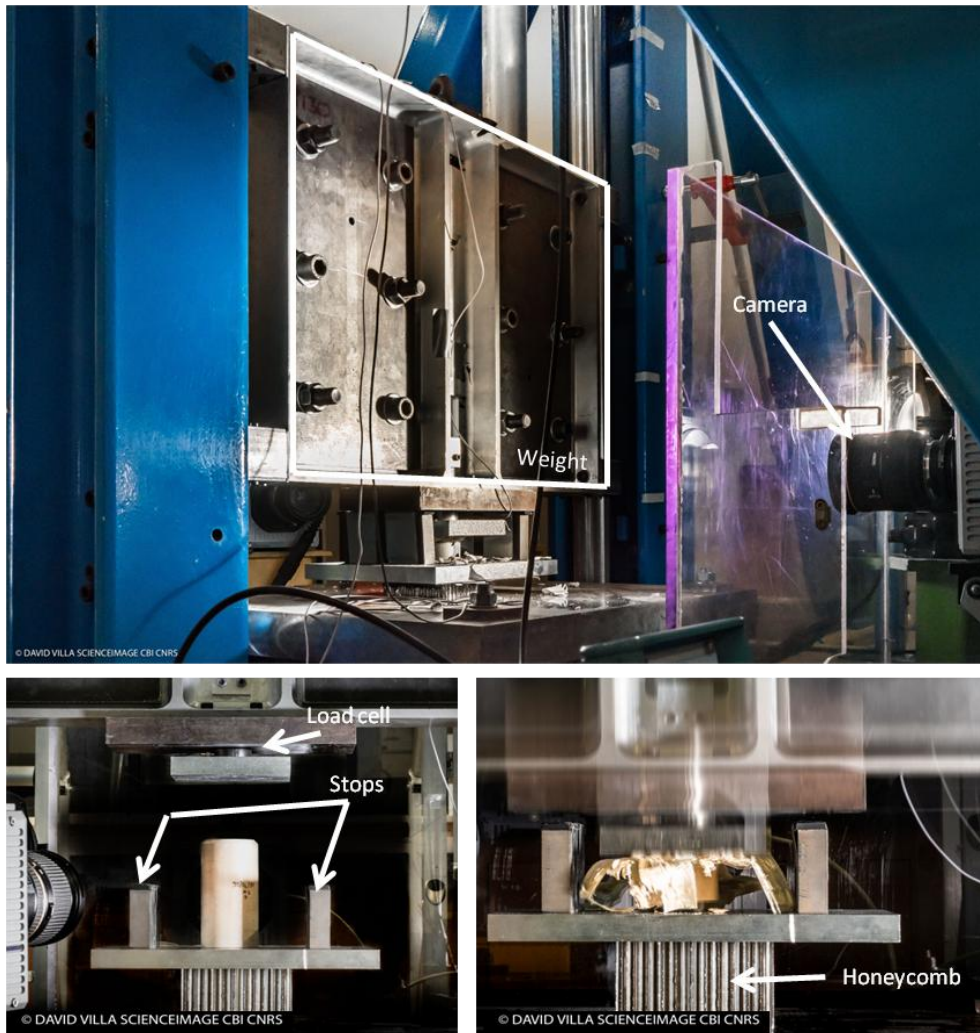


Fig. 2: Drop tower test device for dynamic crushing

103 From the force-displacement curve obtained during the crush, several quantities and performance
104 criteria were extracted. The peak effort is noted F_{\max} . The average effort in the plateau is called F_{plateau} .
105 The CFE (Crush Force Efficiency) is the ratio between the average effort and the maximum effort
106 ($F_{\text{plateau}}/F_{\max}$).

107 In general, when designing a shock absorber, a CFE very close to 1 is desirable, to limit the forces in
108 the rest of the structure during a crash. The energy absorbed here was calculated only on the first 80
109 mm crushed and is noted $EA_{\text{tot}_80\text{mm}}$. It was thus possible to compare static and dynamic crushing even
110 though the dynamic crushing lengths varied somewhat. Finally the SEA was also defined on the first 80
111 millimetres crushed and was therefore calculated as follows: $SEA_{\text{tot}_80\text{mm}} = \frac{F_{\text{tot}_80\text{mm}}}{\rho \times S}$ (J/g), with ρ
112 the average density of the tube (prepreg + glue + veneers) and S the section.

113

114 3. Results and discussion

115 3.1. Sandwich tubes with carbon skins

116 The average crushing speed obtained from the falling weight tests was 8.8 m/s. The dynamic crushing
117 curves are shown in Fig. 3.

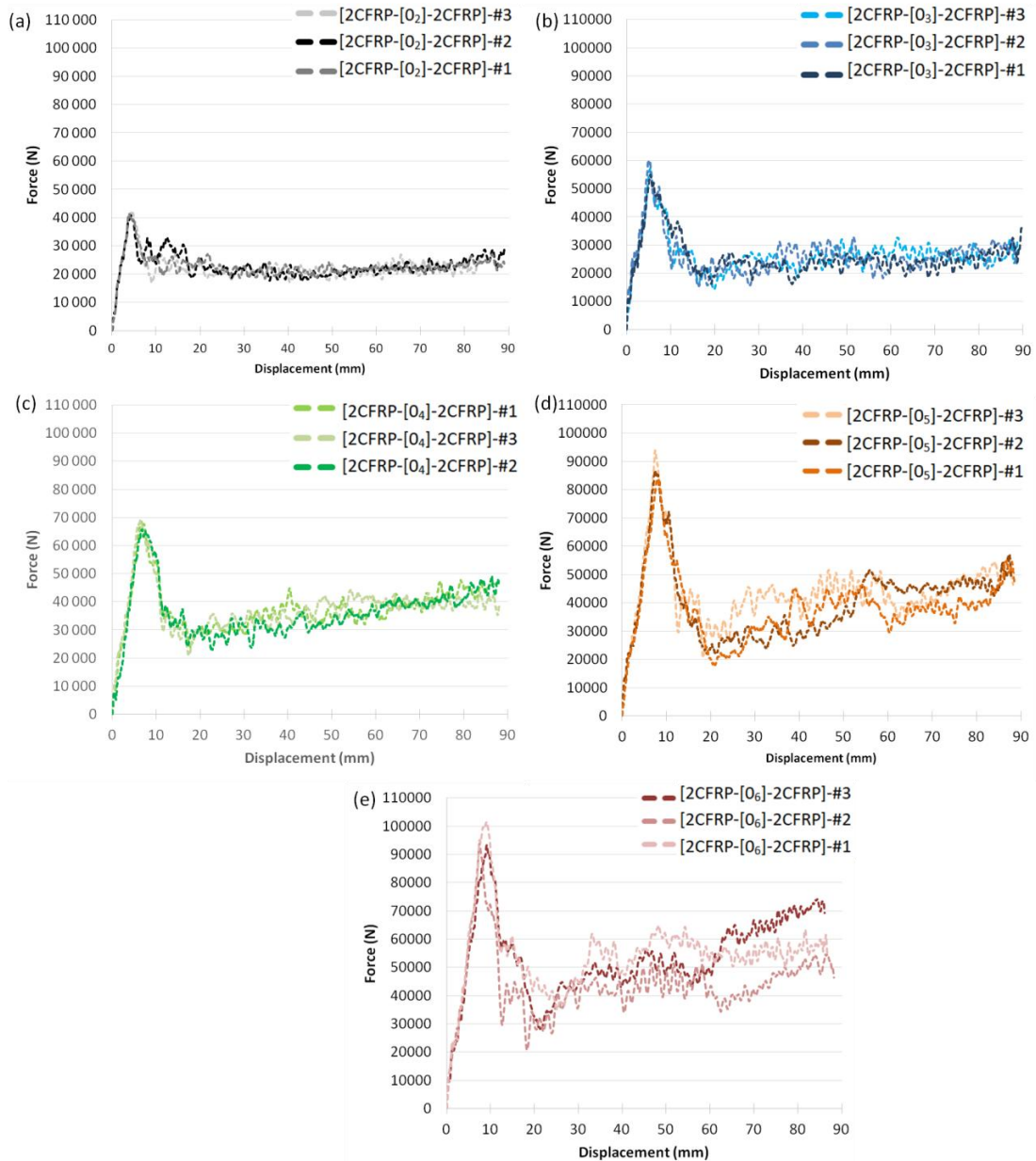


Fig. 3: Dynamic force-displacement curves of tubes (a) [2CFRP-[0₂]-2CFRP] (b) [2CFRP-[0₃]-2CFRP] (c) [2CFRP-[0₄]-2CFRP] (d) [2CFRP-[0₅]-2CFRP] (e) [2CFRP-[0₆]-2CFRP]

The typical phases are visible: initiation, transition and plateau. For tubes with four, five or six l214 plies, the plateau rises as the crushing advances. As the internal compaction of the debris occurs over the same internal diameter, the more the number of l214 plies increases, the more the compaction participates in crushing (Fig. 6). The dynamic performances are presented in Tab. 2.

| | Mass g | Thickness mm | F _{max} N | L _{plateau} mm | F _{plateau} N | CFE | EA _{tot_80mm} J | SEA _{tot_80mm} J/g |
|--------------------------------------|-----------|-----------------|-----------------------|----------------------------|---------------------------|------|-----------------------------|--------------------------------|
| [2CFRP-[0 ₂]-2CFRP] - #1 | 49.0 | 2.93 | 41 389 | 81.4 | 20 440 | 0.49 | 1 718 | 54.3 |
| [2CFRP-[0 ₂]-2CFRP] - #2 | 49.2 | 2.98 | 40 825 | 82.6 | 22 723 | 0.56 | 1 807 | 54.4 |
| [2CFRP-[0 ₂]-2CFRP] - #3 | 49.1 | 2.92 | 42 067 | 80.4 | 21 782 | 0.52 | 1 777 | 53.6 |

| | | | | | | | | |
|--------------------------------------|--------------|-------------|---------------|-------------|---------------|-------------|--------------|-------------|
| Average | 49.1 | 2.94 | 41 427 | 81.5 | 21 649 | 0.52 | 1 767 | 54.1 |
| Standard deviation | 0.1 | 0.03 | 622 | 1.1 | 1 147 | 0.03 | 45 | 0.5 |
| [2CFRP-[0 ₃]-2CFRP] - #1 | 61.8 | 4.34 | 54 968 | 74.3 | 23 739 | 0.43 | 2 020 | 48.1 |
| [2CFRP-[0 ₃]-2CFRP] - #2 | 61.8 | 4.35 | 60 158 | 78.6 | 24 871 | 0.41 | 2 079 | 49.4 |
| [2CFRP-[0 ₃]-2CFRP] - #3 | 61.1 | 4.27 | 57 269 | 78.4 | 25 153 | 0.44 | 2 110 | 50.8 |
| Average | 61.6 | 4.32 | 57 465 | 77.1 | 24 588 | 0.43 | 2 070 | 49.4 |
| Standard deviation | 0.4 | 0.04 | 2 601 | 2.4 | 749 | 0.01 | 46 | 1.3 |
| [2CFRP-[0 ₄]-2CFRP] - #1 | 75.7 | 5.20 | 68 481 | 75.7 | 36 682 | 0.54 | 2 948 | 57.1 |
| [2CFRP-[0 ₄]-2CFRP] - #2 | 75.1 | 5.23 | 65 819 | 76.3 | 35 040 | 0.53 | 2 812 | 54.8 |
| [2CFRP-[0 ₄]-2CFRP] - #3 | 75.2 | 5.19 | 69 228 | 77.2 | 36 140 | 0.52 | 2 983 | 58.1 |
| Average | 75.3 | 5.21 | 67 843 | 76.4 | 35 954 | 0.53 | 2 915 | 56.7 |
| Standard deviation | 0.3 | 0.02 | 1 792 | 0.7 | 837 | 0.01 | 90 | 1.7 |
| [2CFRP-[0 ₅]-2CFRP] - #1 | 91.8 | 6.37 | 93 836 | 75.5 | 42 392 | 0.45 | 3 457 | 54.8 |
| [2CFRP-[0 ₅]-2CFRP] - #2 | 90.9 | 6.50 | 86 722 | 74.6 | 37 819 | 0.44 | 3 132 | 50.1 |
| [2CFRP-[0 ₅]-2CFRP] - #3 | 88.9 | 6.44 | 83 816 | 73.4 | 36 083 | 0.43 | 2 996 | 49.0 |
| Average | 90.5 | 6.44 | 88 125 | 74.5 | 38 765 | 0.44 | 3 195 | 51.3 |
| Standard deviation | 1.5 | 0.07 | 5 155 | 1.1 | 3 259 | 0.01 | 237 | 3.1 |
| [2CFRP-[0 ₆]-2CFRP] - #1 | 102.0 | 7.51 | 101 383 | 74.3 | 53 462 | 0.53 | 4 342 | 61.5 |
| [2CFRP-[0 ₆]-2CFRP] - #2 | 101.9 | 7.50 | 100 587 | 71.8 | 50 729 | 0.50 | 4 178 | 59.3 |
| [2CFRP-[0 ₆]-2CFRP] - #3 | 102.3 | 7.65 | 93 427 | 73.6 | 53 184 | 0.57 | 4 185 | 59.2 |
| Average | 102.1 | 7.52 | 98 466 | 73.2 | 52 459 | 0.53 | 4 235 | 60.0 |
| Standard deviation | 0.2 | 0.03 | 4 382 | 1.3 | 1 504 | 0.03 | 93 | 1.3 |

Tab. 2: Results for dynamic crushing of [2CFRP-[0_n]-2CFRP]_{2 ≤ n ≤ 6}

125

126

127

128

129

130

The failure mode of this configuration is initiated by the flattening of the chamfer in contact with the crushing plate. The outer and inner skins then come into contact with the platter and are then forced to splay inwards and outwards. The deformation imposed on the fibres oriented at 90° causes them to break and allows the tube to dissociate into bundles. As the crushing continues, the bundles and splaying of the inner and outer skins create petals (Fig. 4).

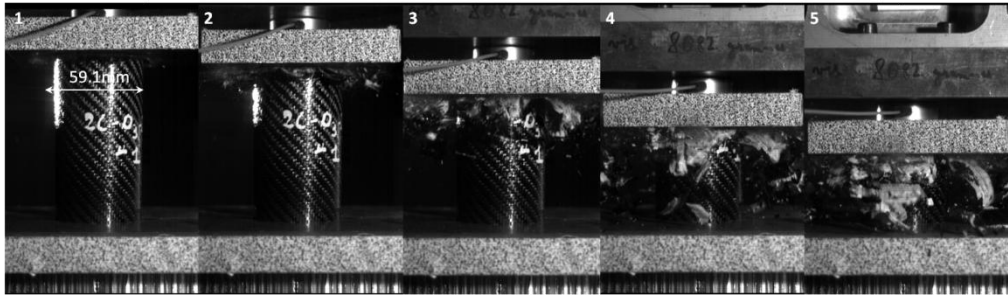
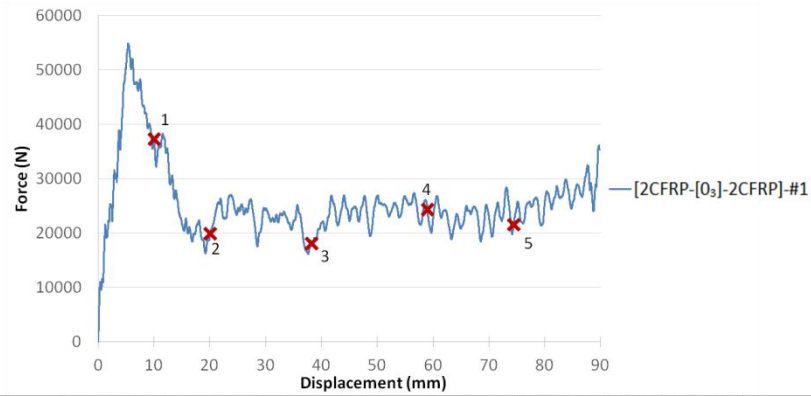


Fig. 4: Dynamic failure of tube [2CFRP-[0₃]-2CFRP]-#1 and association of pictures and points on the force displacement curve.

Post-crash analysis of the tubes shows fairly significant debris compaction within the tube (Fig. 5).

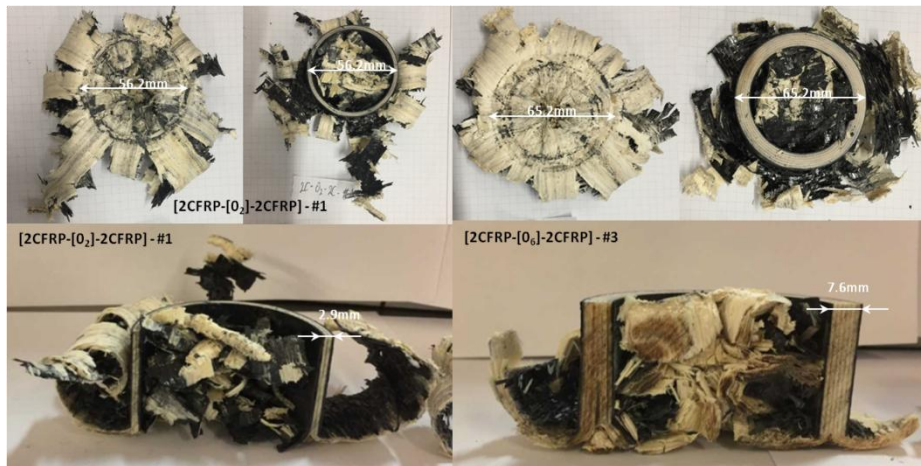


Fig. 5: Dynamic destruction of tubes [2CFRP-[0₂]-2CFRP]-#1 and [2CFRP-[0₆]-2CFRP]-#3 and of ½ tubes [2CFRP-[0₃]-2CFRP]-#3 and [2CFRP-[0₄]-2CFRP]-#1

The tubes have a generally similar failure mode but it is difficult to establish a link between the performance drops of configurations with different numbers of I214 plies and the differences in failure modes: the same configuration can present different failure patterns (Fig. 6), a common item for issue in crash testing.

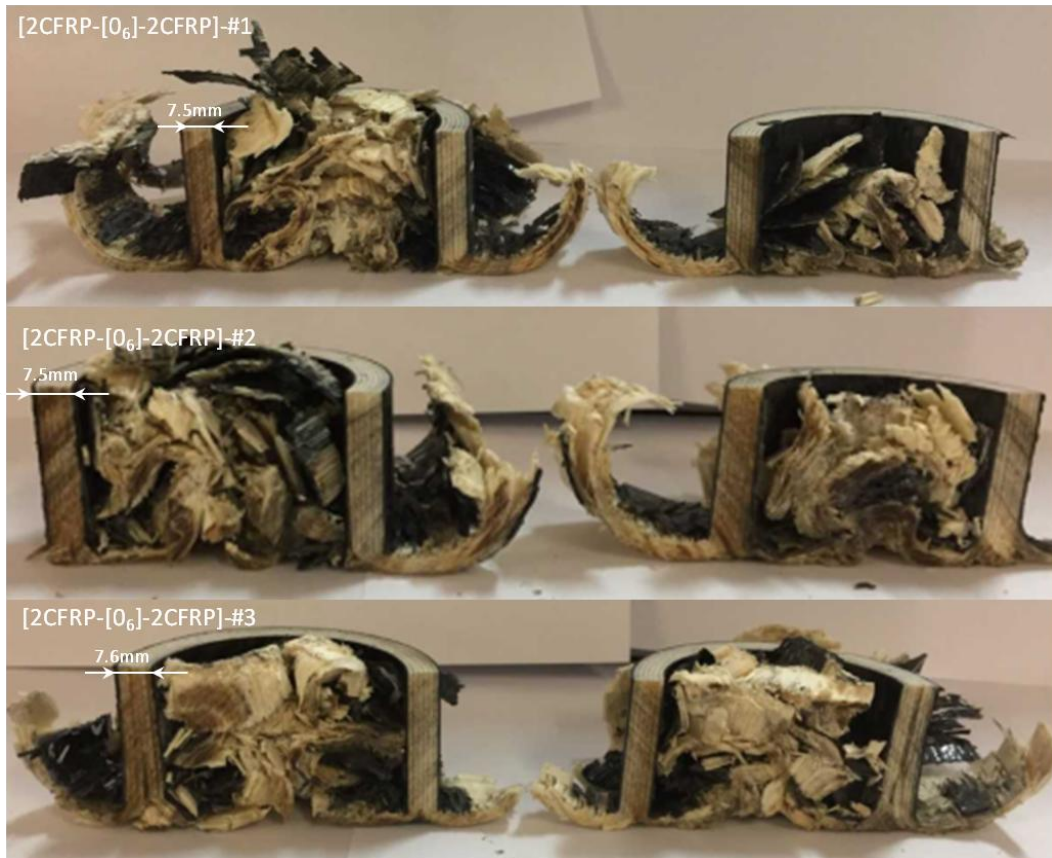


Fig. 6: Post-crush patterns of half sandwich tubes [2CFRP-[0₆]-2CFRP].

142

143

144 Here, for the [2CFRP-[0₆]-2CFRP] configuration, which shows good repeatability (Tab. 2) between these
 145 tubes, the failure mode is generally similar but there are differences, e.g. different central cracking
 146 position. Moreover, on the same tube, it can be seen that the failure front changes between the two half-
 147 tubes: [2CFRP- [0₆]-2CFRP] # 2, for example, exhibits one wall with bending over its entire 'thickness
 148 while the other wall is divided into two inner and outer parts an inner and an outer part.

149 Absorbed energy and SEA are plotted versus the number of folds in Fig. 7 (a). As splaying and
 150 internal debris compaction constitute the overall ruin mechanism of each ply configuration, the peak
 151 load and mean crush force at the plateau are plotted as a function of the section of the tubes in Fig. 7.

152 (b).

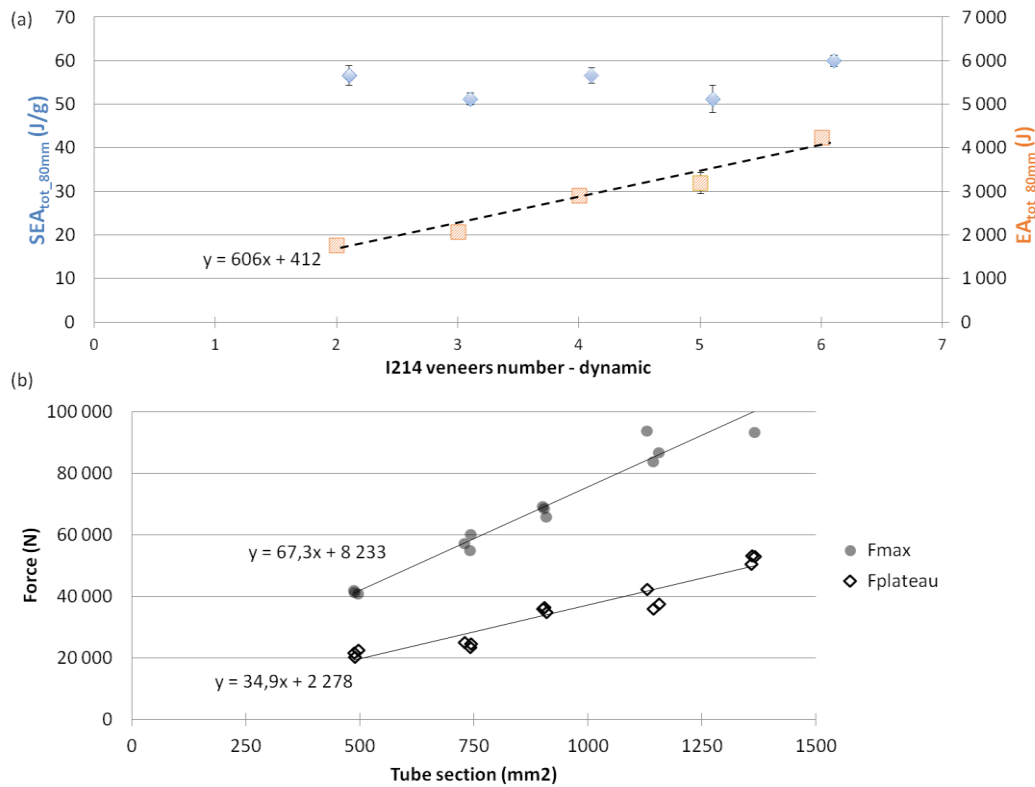


Fig. 7: (a) Evolution of EA_{tot_80mm} and SEA_{tot_80mm} versus the number of I214 layers. (b) Maximum and plateau force versus tube sections for tubes with carbon skins.

153
154
155

156 The energy absorbed increases linearly with the number of I214 folds, as expressed by the equation
 157 $EA_{tot_80mm} = 606 \times \text{number of layers}_{I214} + 412$, with 606 J which would represent the
 158 contribution of a single I214 poplar layer and 412 J the contribution of carbon skins. On average, the
 159 SEA oscillates between 48.1 J / g for the lowest value ([2CFRP-[0₃]-2CFRP]) and 61.5 J/g ([2CFRP-[0₆]-
 160 2CFRP]).

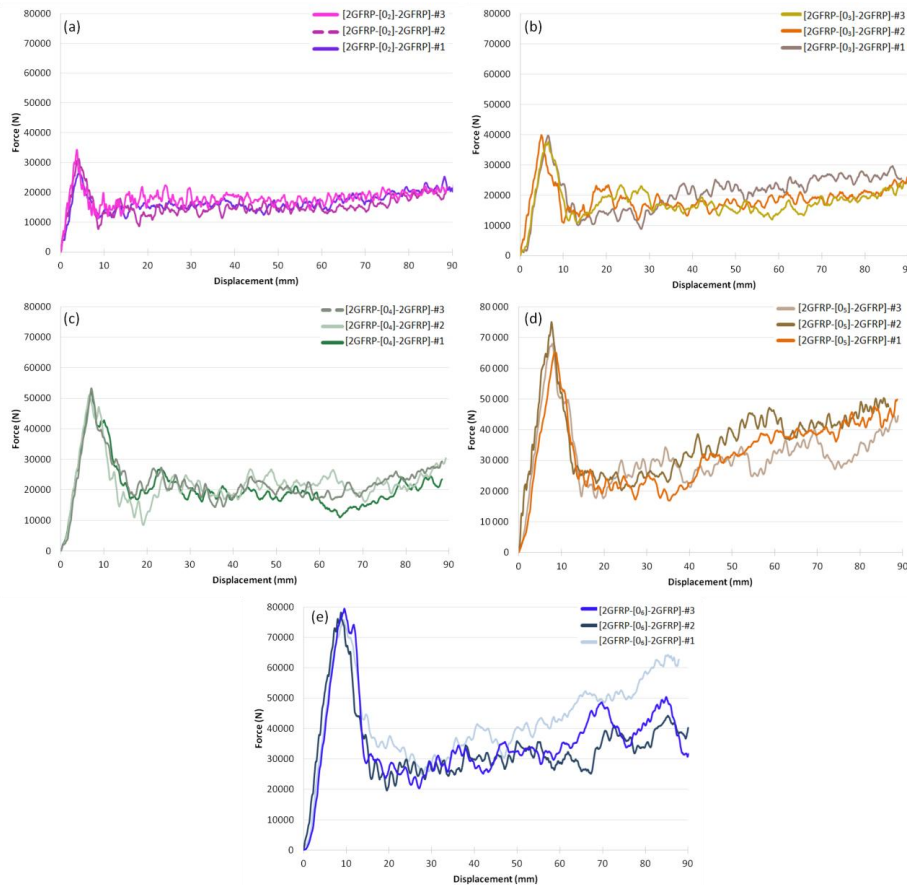
161 The peak load and the mean crushing force increases linearly with the section. The load peaks are
 162 higher than the average forces, the difference depending on the section of the tubes **OK?**. This is due to
 163 a more efficient failure mechanism during the loading phase than during the plateau phase. The
 164 equation of these two quantities confirms that the carbon fibre skins and the I214 plies work more
 165 efficiently in the loading phase than in the plateau phase: 67.3 MPa for the I214 layers and 8 233 N for
 166 the carbon skins versus 34.9 MPa and 2278 N respectively. The average crush stress of an I214 ply
 167 corresponds to overall failure mechanisms such as splaying and internal debris compaction and is 34.9
 168 MPa.

169

170 3.2. Sandwich tubes with glass skins

171 The average crushing speed obtained from the falling weight tests was 8.4 m/s. The dynamic crushing

172 curves are shown in Fig. 8.



173

174 Fig. 8: Dynamic force-displacement curves for tubes (a) [2GFRP-[0₂]-2GFRP] (b) [2GFRP-[0₃]-2GFRP] (c) [2GFRP-
175 [0₄]-2GFRP] (d) [2GFRP-[0₅]-2GFRP] (e) [2GFRP-[0₆]-2GFRP]

176 Again, the three phases (initiation, transition and plateau) are found. As with the sandwich tubes with

177 carbon skins, for five and six layers of poplar, the crushing force is no longer constant and rises in the

178 plateau phase as the crushing increases. The compaction of the interior debris may be responsible for

179 this rise. The peak load, the plateau force and, therefore, the energy absorbed increase with the number

180 of l214 layers, (Tab. 3).

181

| | g | mm | N | mm | N | / | J | J/g |
|--------------------------------------|------|-----------|------------------|----------------------|----------------------|------|------------------------|------------------------|
| | Mass | Thickness | F _{max} | L _{plateau} | F _{plateau} | CFE | EA _{tot_80mm} | SEA _{plateau} |
| [2GFRP-[0 ₂]-2GFRP] - #1 | 46.5 | 2.86 | 26 574 | 82.0 | 16 725 | 0.63 | 1 284 | 42.8 |
| [2GFRP-[0 ₂]-2GFRP] - #2 | 47.9 | 2.99 | 31 163 | 82.3 | 14 695 | 0.47 | 1 203 | 36.5 |

| | | | | | | | | |
|--------------------------------------|--------------|-------------|---------------|-------------|---------------|-------------|--------------|-------------|
| [2GFRP-[0 ₂]-2GFRP] - #3 | 48.0 | 2.90 | 34 353 | 82.3 | 17 956 | 0.52 | 1 428 | 44.4 |
| Average | 47.5 | 2.92 | 30 697 | 82.2 | 16 459 | 0.54 | 1 305 | 41.2 |
| Standard deviation | 0.8 | 0.07 | 3 910 | 0.2 | 1 647 | 0.08 | 114 | 4.2 |
| [2GFRP-[0 ₃]-2GFRP] - #1 | 58.4 | 4.25 | 39 771 | 75.0 | 20 827 | 0.53 | 1 612 | 40.8 |
| [2GFRP-[0 ₃]-2GFRP] - #2 | 58.1 | 3.98 | 39 910 | 79.7 | 18 221 | 0.46 | 1 462 | 37.2 |
| [2GFRP-[0 ₃]-2GFRP] - #3 | 59.6 | 4.11 | 37 706 | 77.7 | 17 228 | 0.46 | 1 388 | 34.4 |
| Average | 58.7 | 4.11 | 39 129 | 77.5 | 18 759 | 0.48 | 1 487 | 37.5 |
| Standard deviation | 0.8 | 0.14 | 1 234 | 2.4 | 1 859 | 0.04 | 114 | 3.2 |
| [2GFRP-[0 ₄]-2GFRP] - #1 | 71.6 | 5.22 | 52 201 | 72.2 | 18 713 | 0.36 | 1 647 | 33.8 |
| [2GFRP-[0 ₄]-2GFRP] - #2 | 71.6 | 5.11 | 51 071 | 75.9 | 21 046 | 0.41 | 1 760 | 36.1 |
| [2GFRP-[0 ₄]-2GFRP] - #3 | 71.9 | 5.05 | 53 294 | 72.1 | 21 229 | 0.40 | 1 774 | 36.3 |
| Average | 71.7 | 5.13 | 52 189 | 73.4 | 20 329 | 0.39 | 1 727 | 35.4 |
| Standard deviation | 0.2 | 0.09 | 1 112 | 2.1 | 1 403 | 0.03 | 70 | 1.4 |
| [2GFRP-[0 ₅]-2GFRP] - #1 | 85.2 | 6.09 | 65 266 | 74.8 | 31 963 | 0.49 | 2 512 | 41.8 |
| [2GFRP-[0 ₅]-2GFRP] - #2 | 90.2 | 6.32 | 75 043 | 73.8 | 35 359 | 0.47 | 2 856 | 46.2 |
| [2GFRP-[0 ₅]-2GFRP] - #3 | 87.9 | 6.28 | 68 083 | 74.4 | 29 835 | 0.44 | 2 448 | 42.1 |
| Average | 87.8 | 6.23 | 69 464 | 74.3 | 32 386 | 0.47 | 2 605 | 43.3 |
| Standard deviation | 2.5 | 0.12 | 5 032 | 0.5 | 2 786 | 0.03 | 220 | 2.5 |
| [2GFRP-[0 ₆]-2GFRP] - #1 | 104.3 | 7.54 | 75 750 | 74.7 | 42 479 | 0.56 | 3 291 | 45.8 |
| [2GFRP-[0 ₆]-2GFRP] - #2 | 102.5 | 7.24 | 78 173 | 74.3 | 31 219 | 0.40 | 2 648 | 37.6 |
| [2GFRP-[0 ₆]-2GFRP] - #3 | 104.4 | 7.38 | 79 540 | 75.9 | 33 778 | 0.42 | 2 787 | 38.8 |
| Average | 103.7 | 7.39 | 77 821 | 75.0 | 35 825 | 0.46 | 2 908 | 40.7 |
| Standard deviation | 1.1 | 0.15 | 1 920 | 0.8 | 5 902 | 0.09 | 338 | 4.4 |

Tab. 3: Results for dynamic crushing of [2GFRP-[0_n]-2GFRP]_{2≤n≤6}

182

183

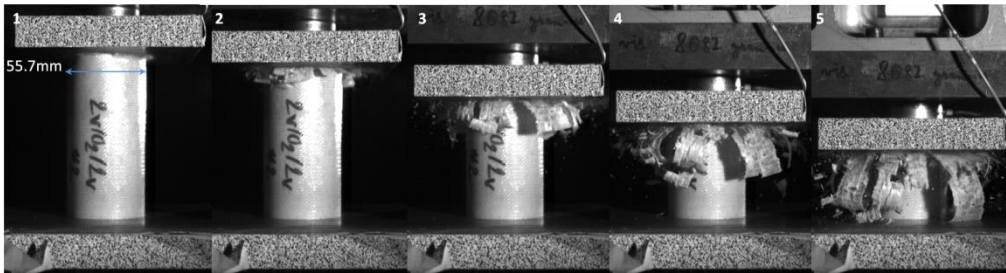
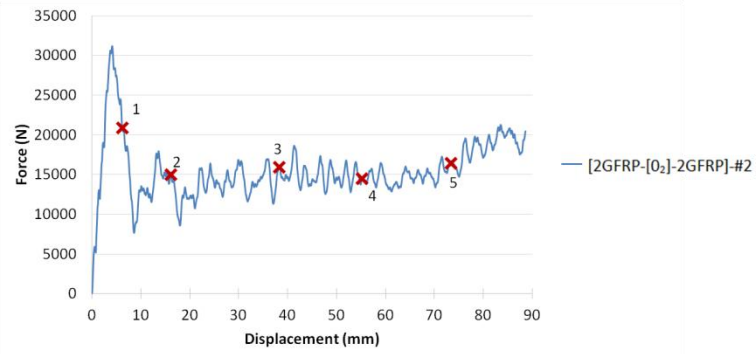
184

185

186

187

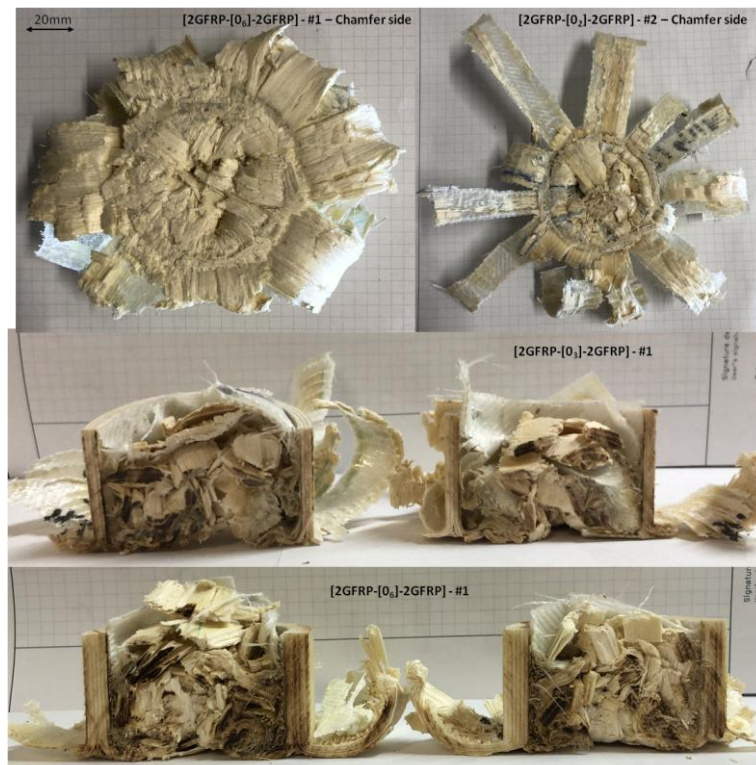
The failure mode is rather similar to that of the tubes with carbon fibre skins. In fact, in contact with the crushing plate, the chamfer flattens out, introducing enough deformation of the glass fibres oriented at 90° to force them to break. By breaking, they dissociate the tube into bundles and allow a splaying of the inner and outer skins as well as the I214 layers (Fig. 9).



188
189
190 Fig. 9: Dynamic failure of tube [2GFRP-[0₂]-2GFRP]-#2 and association of pictures and points on the force/ displacement curve.

191 The dissociation into bundles of the tube, accompanied by the splaying, leads to the formation of petals.

192 Fairly significant compaction was observed inside the tube (Fig. 10).

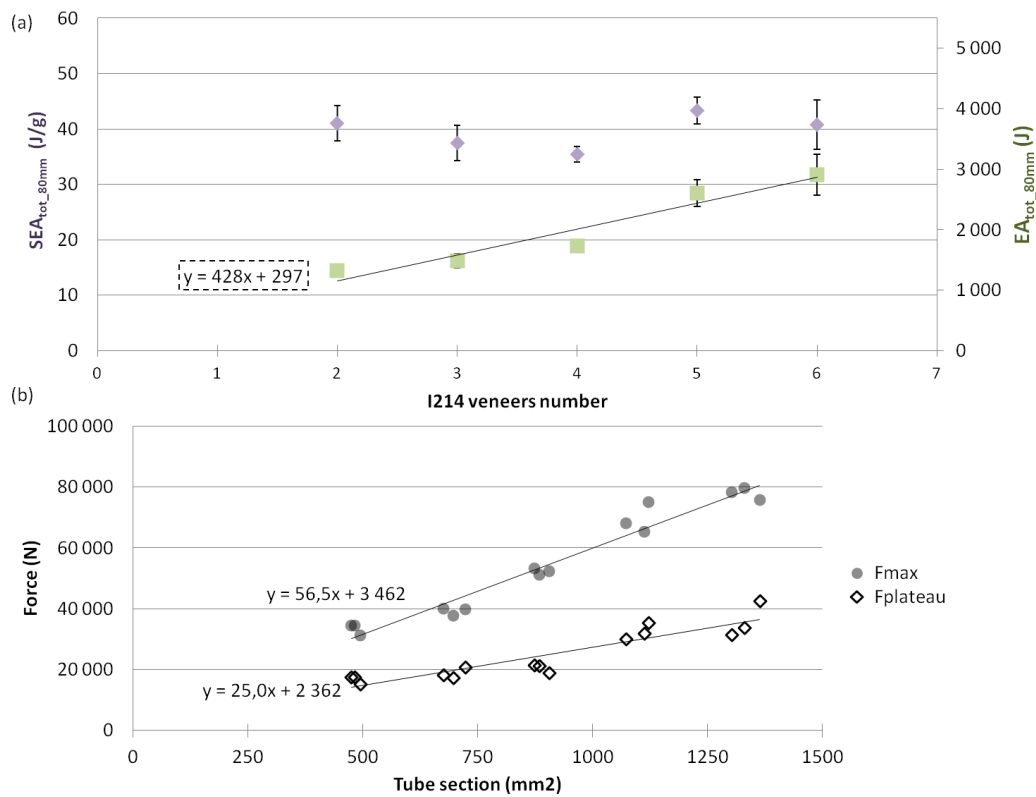


193
194
195 Fig. 10: Dynamic failure of tubes [2GFRP-[0₂]-2GFRP]-#1 and [2GFRP-[0₆]-2GFRP]-#1, and ½ tubes [2GFRP-[0₃]-2GFRP]-#1 and [2GFRP-[0₆]-2GFRP]-#1.

196 A slight debonding of the inner and outer skin and the I214 layers was also observed. Although the

197 energy absorbed varied almost linearly with the number of I214 plies used, SEA was not constant (Fig.

198 11 (a)). As the failure mechanisms were similar between the I214 ply configurations, the peak effort and
 199 the mean effort at the plateau level were plotted versus the section of the tubes (Fig. 11 (b)).



200
 201 **Fig. 11: Evolution of EA_{tot_80mm} and SEA_{tot_80mm} versus the number of I214 layers. (b) Maximum and plateau force**
 202 **versus tube sections for tubes with glass skins.**

203 The increase in the energy absorbed for the three- and four-layer configuration was not significantly high
 204 compared to the increase in the mass of the sandwich and, therefore, the SEA decreased from 40.8 J /
 205 g on average to 37.5 then 35.4 J / g. The same observation was made for configurations with five and
 206 six poplar layers, where the absorbed energy gained thanks to the additional poplar layers was
 207 insufficient to give a gain in SEA. The differences in SEA between the configurations having three and
 208 four layers are difficult to explain. As with CFRP tubes, it was observed on several tubes that the failure
 209 front could have a different number of I214 folds splayed towards the inside of the tube on the same
 210 plane. As the energy absorbed increases linearly with the number of I214 folds, it can be represented
 211 by: $EA_{tot_80mm} = 428 \times number\ layer_{I214} + 297$, where 428 J is the contribution of each I214
 212 layer and 297 J the contribution of the glass fibre skins. As with carbon fibre skins, the failure

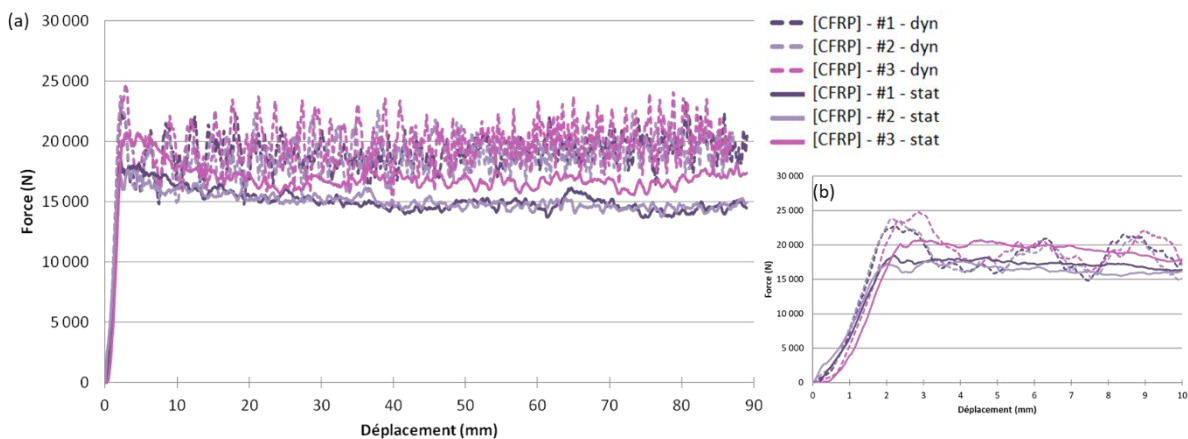
213 mechanisms were more efficient in the loading phase than in the plateau phase. The average crushing
 214 stress of an I214 ply surrounded by glass fibres was 25 MPa.

215

216 3.3. Comparison between static and dynamic crushes

217 3.3.1. Tubes with carbon skins.

218 In this part, the static and dynamic performances obtained on the configuration [2CFRP-[0_N]-
 219 2CFRP]_{2≤N≤6} are compared. But, first, the crushes of CFRP monolithic tubes with 4 carbon layers (Fig.
 220 12) are studied in order to see the influence of the static and dynamic behaviour of wood coupled to
 221 carbon fibres. The crushing of the CFRP tubes was carried out at the same speed as the crushing of the
 222 sandwich tubes (8.8 m / s).



223
 224

Fig. 12: (a) Static and dynamic crushing of tubes with carbon skins, (b) Zoom on initiation.

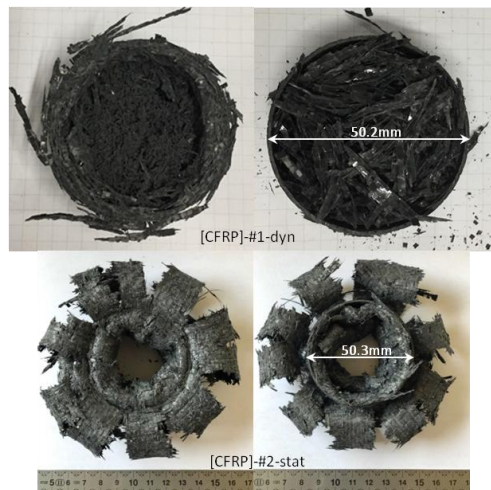
225 Again, the three crushing phases were found in both statics and dynamics. The oscillations were much
 226 greater in dynamics than in statics, even though no filtering was applied. The performances (Tab. 4)
 227 showed a slightly higher peak load in dynamic than in static configuration but the CFE was not degraded
 228 because the plateau also increased in dynamic tests and gave a CFE of 0.82 in dynamic and 0.80 in
 229 static.

| | | Mass | Thickness | F _{max} | L _{plateau} | F _{plateau} | CFE | EA _{tot_80mm} | SEA _{tot_80mm} |
|-------------|----------------|-------------|-------------|------------------|----------------------|----------------------|-------------|------------------------|-------------------------|
| | | g | mm | N | mm | N | | J | J/g |
| Static test | CFRP - I | 27.7 | 0.97 | 18 434 | 79.2 | 14 942 | 0.81 | 1 203 | 64.6 |
| | CFRP - II | 27.9 | 0.97 | 17 603 | 80.7 | 14 947 | 0.85 | 1 196 | 63.7 |
| | CFRP - III | 27.6 | 0.97 | 20 729 | 79.3 | 16 821 | 0.81 | 1 340 | 71.8 |
| | Average | 27.7 | 0.97 | 18 922 | 79.7 | 15 570 | 0.82 | 1 247 | 66.7 |

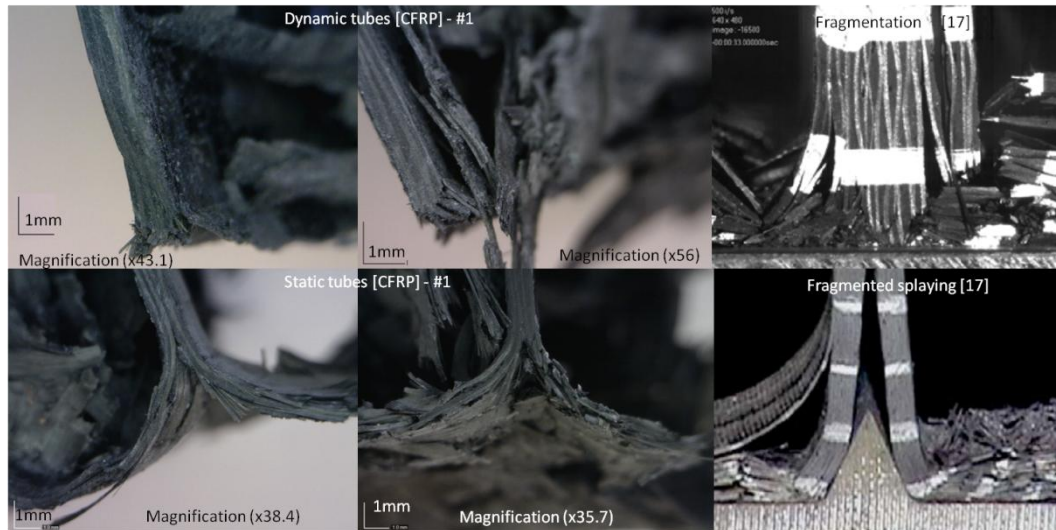
| | Standard deviation | 0.2 | 0.00 | 1 619 | 0.8 | 1 083 | 0.02 | 81 | 4.5 |
|--------------|---------------------------|-------------|-------------|---------------|-------------|---------------|-------------|--------------|-------------|
| Dynamic test | CFRP - I | 27.5 | 0.97 | 23 232 | 85.6 | 19 060 | 0.82 | 1 499 | 80.9 |
| | CFRP - II | 27.7 | 0.99 | 23 783 | 82.9 | 18 897 | 0.79 | 1 491 | 79.8 |
| | CFRP - III | 27.7 | 0.97 | 24 780 | 84.0 | 19 789 | 0.80 | 1 557 | 83.2 |
| | Average | 27.6 | 0.98 | 23 932 | 84.2 | 19 249 | 0.80 | 1 516 | 81.3 |
| | Standard deviation | 0.1 | 0.01 | 785 | 1.3 | 475 | 0.01 | 36 | 1.7 |

230 **Tab. 4: Results for static and dynamic crush of monolithic [CFRP] tubes.**

231 The gain in specific energy absorption in dynamic tests was 14.6 J/g. The dynamic performance of
 232 carbon tubes was thus higher than in the static situation. The failure mode between statics and
 233 dynamics was also different. In static conditions, the damage was caused by the progressive formation
 234 of petals via splaying (Fig. 13). In dynamics, the post-mortem observation did not reveal whether the
 235 numerous debris generated during the test were created by splaying or by fragmentation. Viewing the
 236 videos obtained by the fast cameras did not decide this point either. The [CFRP] tubes were therefore
 237 cut in half in order to observe the failure front under the microscope (Fig. 14).



238 **Fig. 13: Static and dynamic [CFRP] post-mortem failure pattern (chamfered side of the tube: photo on left; top of the**
 239 **tube: photo on right)**
 240

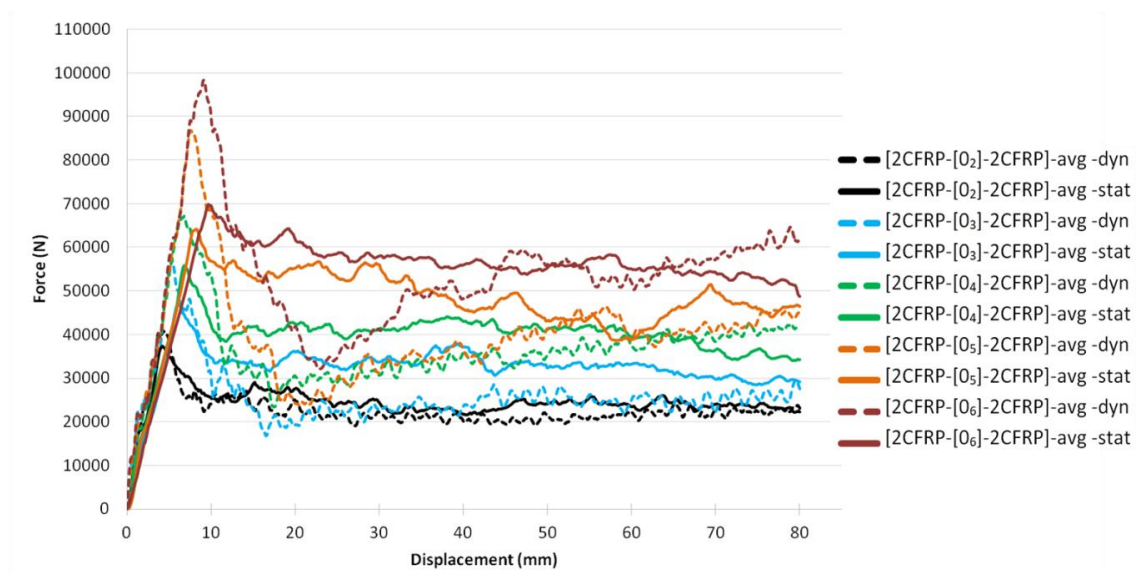


241
242
243

Fig. 14: Comparison of static and dynamic failure patterns of [CFRP] tube via microscopic observation (Right from [31]).

244 The static front shows splaying accompanied by failures in the laminate similar to the failure mode
245 obtained by Guillon and called fragmented splaying [31]. Concerning the dynamic failure front, the
246 absence of central cracking indicates more a classical dynamic failure mode of fragmentation which can
247 be explained by a more fragile behaviour of the carbon fibres or the matrix with the increase in the strain
248 rate.

249 Now, the results for the sandwich tubes are discussed. The averaged $[2CFRP-[0_N]-2CFRP]_{2 \leq N \leq 6}$
250 $[2CFRP-[0_N]-2CFRP]_{2 \leq N \leq 6}$ curves are superimposed in Fig. 15.

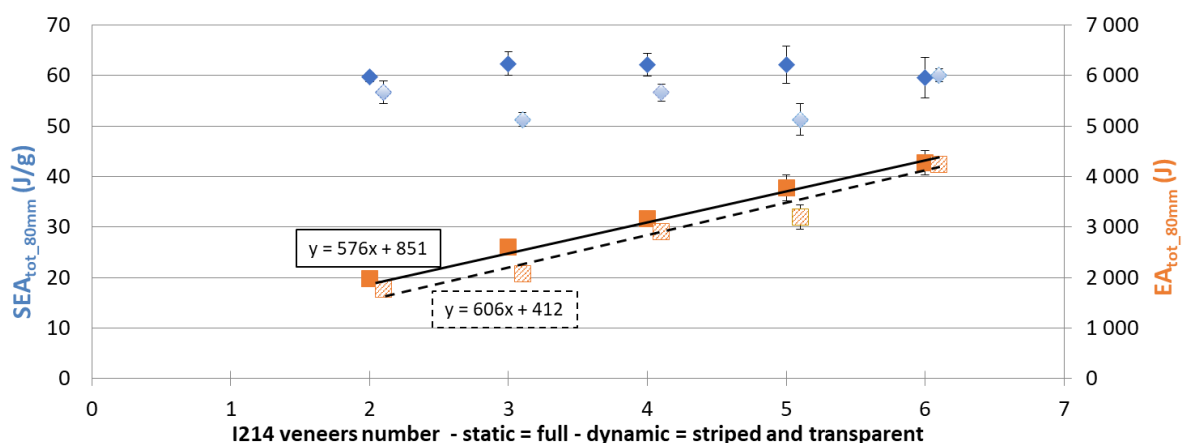


251
252

Fig. 15: Mean dynamic and static force-displacement curves of sandwich tubes $[2CFRP-[0_n]-2CFRP]_{2 \leq n \leq 6}$

253 The peak load is much higher in dynamic than in static (98,466 N for six poplar layers in dynamic versus
 254 70,074 N in static, for example). An examination of the crushing plateau shows that the dynamic levels
 255 are lower than the static in each configuration. Thus, the dynamic CFE (varying from 0.41 to 0.57) is
 256 degraded in comparison to the static (varying from 0.63 to 0.85). The second observation concerns the
 257 transition phase, which differs from dynamic to static. In fact, in dynamics, after the peak load, the force
 258 decreases during about ten millimetres of crushing and then reaches the plateau. The transition phase
 259 is thus longer in dynamics than in statics. In addition, in dynamics, the plateau increases as the crushing
 260 progresses, more particularly for the configurations having four, five or six poplar layers. This is probably
 261 in connection with the compaction of the debris inside the tube, which results in a larger volume of
 262 debris for globally the same overall dimensions of the tube. In both statics and dynamics, the energy
 263 absorbed increased linearly with the number of I214 layers (Fig. 17). The equation shows that the
 264 contribution of a wood ply is slightly greater in dynamics (606 J) than in statics (576 J). The y-intercept
 265 provides information on how CFRP skins behave. They can be seen to absorb less energy dynamics
 266 (412 J) than in statics (851 J). In dynamic tests, the CFRP tubes alone absorbed an energy of 1516 J,
 267 showing that they work better on their own than as the skin of sandwich tubes. However, CFRP skins
 268 stabilized the I214 layers oriented at 0° thus improving the crash behaviour of the sandwich. The
 269 average value as a function of the number of I214 layers of the dynamic SEA is also more dispersed
 270 than the static SEA.

271



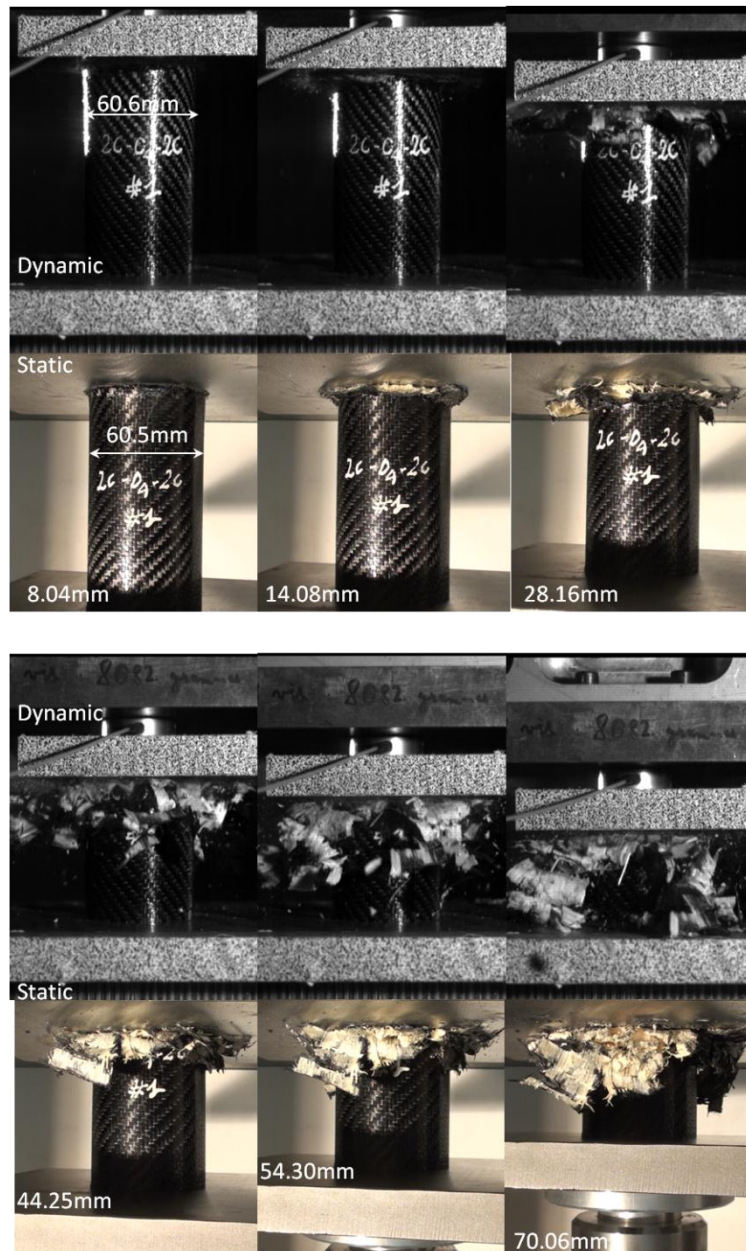
272

273
274

Fig. 16: Evolution of $EA_{tot,80mm}$ and $SEA_{tot,80mm}$ according to the number of I214 plies in static and dynamic for tubes with carbon skins.

275
276
277
278
279
280
281

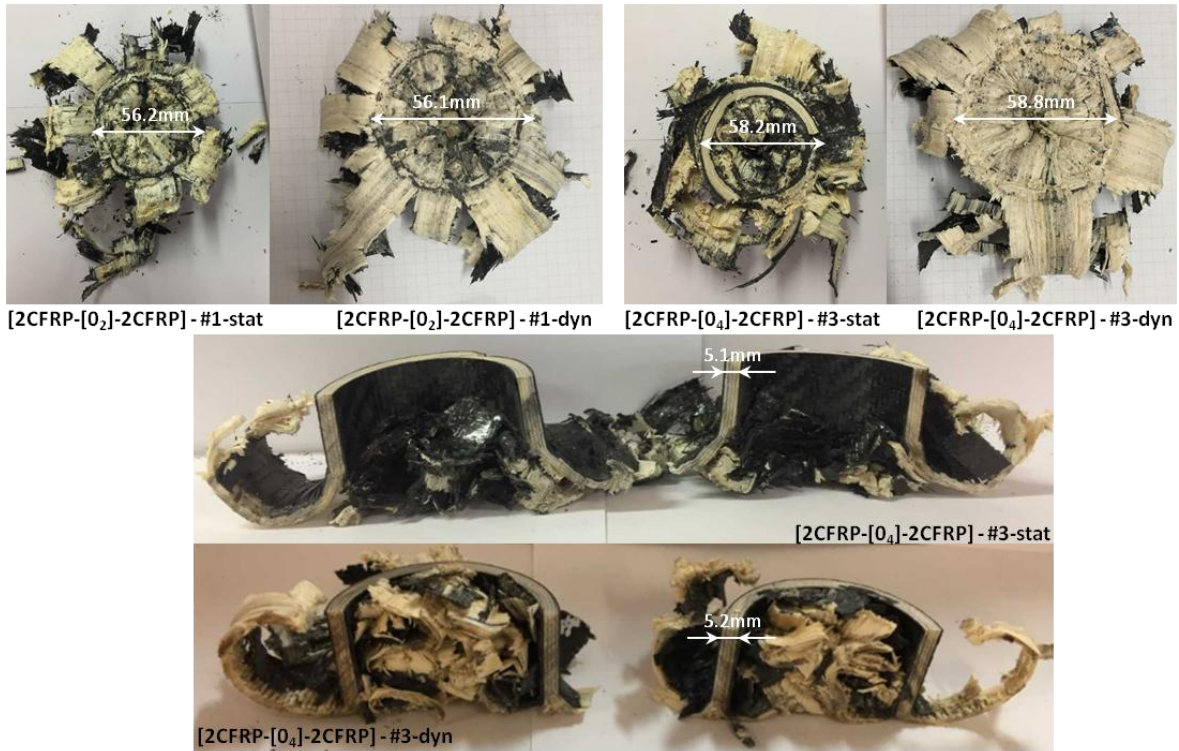
Whether CFE, absorbed energy or SEA is considered, the dynamic performance of these sandwich tubes is slightly lower than their static performance. The average crushing stress with carbon fibre skins is almost identical between the static (37.2 MPa) and dynamic (34.9 MPa) regimes. A comparison of the static and dynamic failure modes shows that the overall failure is similar: splaying with the formation of petals (Fig. 18 and Fig. 19). However, certain phenomena, such as local buckling, are no longer present in the dynamic failure mode. Finally, it should also be noted that the compaction of the debris inside the tube is greater in dynamics (Fig. 19).



282

283
284

Fig. 17: Static and dynamic comparison of the failure mode of the tube [2CFRP-[0₄]-2CFRP]-#1 at iso-displacement (the static images have been turned).



285
286

Fig. 18: Static and dynamic comparison of post-mortem failure patterns for tubes with carbon skins.

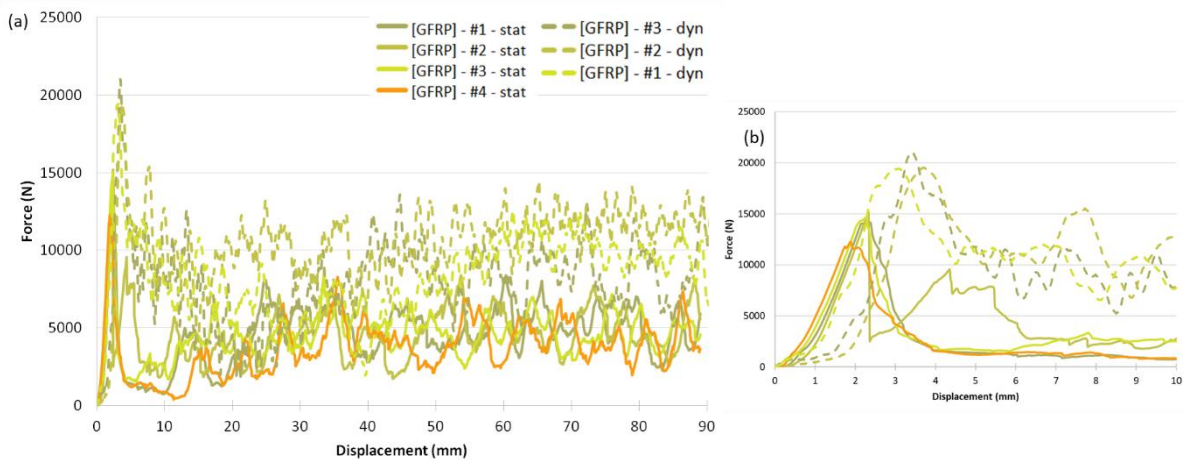
287
288

3.3.2 Tubes with glass skins

289 The static and dynamic performance of the sandwiches [2GFRP-[0_N]-2GFRP]_{2 ≤ N ≤ 6} were compared.

290 First, the crushes of monolithic GFRP tubes with four GFRP layers (Fig. 12) were studied to investigate

291 the influence of the static and dynamic behaviour of wood coupled with carbon fibres.



292
293

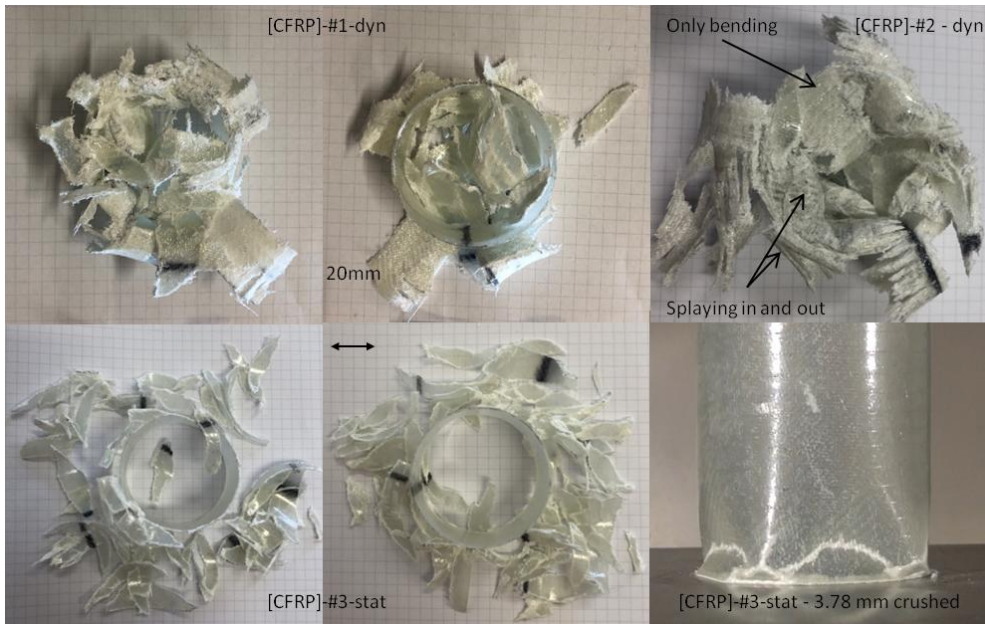
Fig. 19: (a) Static and dynamic crushing of monolithic glass tubes (b) Focus on initiation

294 Once again, the three classical phases were found in static and dynamic. On the overall reading of the
 295 crushing curves, an improvement in the energy absorption capacities of the dynamic glass fibre tubes
 296 was observed. The average plateau force was almost doubled, resulting in the doubling of the energy
 297 absorbed and the SEA (Tab. 5).

| | | Mass g | Thickness mm | F _{max} N | L _{plateau} mm | F _{plateau} N | CFE / | EA _{tot_80mm} J | SEA _{tot_80mm} J/g |
|---------------|---------------------------|---------------------------|-----------------|-----------------------|----------------------------|---------------------------|--------------|-----------------------------|--------------------------------|
| Static tests | [GFRP] - #1 | 24.2 | 0.65 | 14 179 | 76.0 | 4 860 | 0.34 | 369 | 22.6 |
| | [GFRP] - #2 | 24.3 | 0.68 | 15 178 | 83.3 | 4 476 | 0.29 | 363 | 22.2 |
| | [GFRP] - #3 | 23.7 | 0.67 | 14 617 | 77.5 | 4 674 | 0.32 | 359 | 22.5 |
| | [GFRP] - #4 | 23.7 | 0.67 | 12 275 | 74.7 | 3 985 | 0.32 | 291 | 18.3 |
| | Average | 24.0 | 0.67 | 14 062 | 77.9 | 4 499 | 0.32 | 364 | 21.4 |
| | Standard deviation | 0.3 | 0.01 | 1 260 | 3.8 | 377 | 0.02 | 37 | 2.1 |
| Dynamic tests | [GFRP] - #1 | 24.8 | 0.70 | 19 430 | 88.4 | 8 230 | 0.42 | 656 | 39.6 |
| | [GFRP] - #2 | 25.0 | 0.75 | 19 525 | 87.1 | 10 329 | 0.53 | 793 | 47.5 |
| | [GFRP] - #3 | 25.1 | 0.72 | 21 015 | 85.4 | 7 923 | 0.38 | 632 | 37.8 |
| | Average | 25.0 | 0.72 | 19 990 | 87.0 | 8 827 | 0.44 | 694 | 41.6 |
| | | Standard deviation | 0.1 | 0.03 | 889 | 1.6 | 1 310 | 0.08 | 87 |

298 **Tab. 5: Static and dynamic [GFRP] tube crush results.**

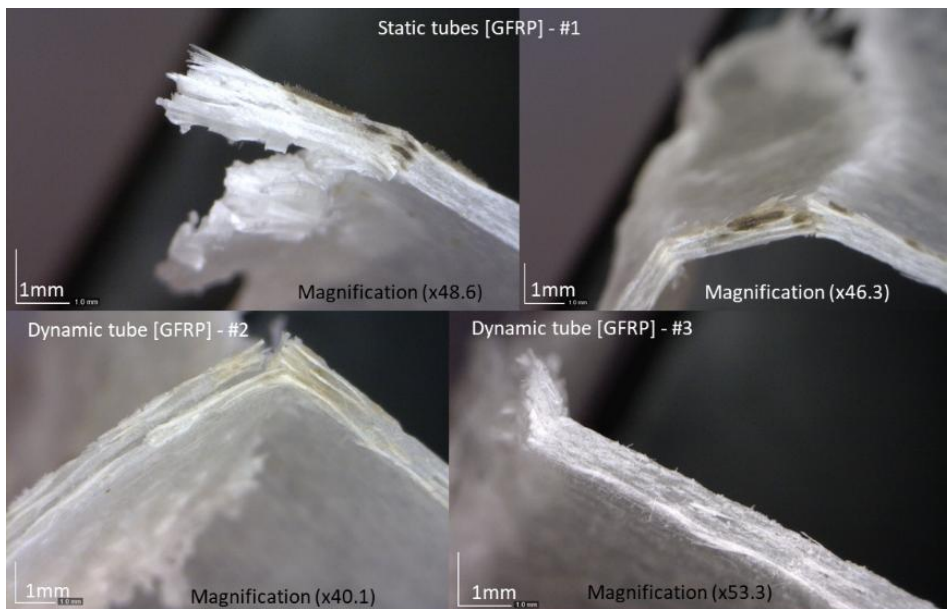
299 The increase in absorbed energy and SEA can be explained by a difference in failure mode between
 300 static and dynamic. During the static crush, large pieces of debris were created (of the order of a few
 301 centimetres) accompanied by instability of the walls of the tube, leading to very little energy absorption.
 302 In dynamics, the size of debris was much smaller (dust was visible on high speed camera images)
 303 although some macroscopic debris was created (Fig. 21). Post-mortem observation of the dynamic
 304 tubes showed the occasional presence of petals that were created by local splaying or via full-thickness
 305 bending.



306
307
308

Fig. 20: Static and dynamic [GFRP] tube post-mortem patterns (chamfered side of the tube: photo on the left; top of the tube: photo on the right)

309 Observation of the thickness of a half-tube [GFRP] under a microscope indicated the absence of a
 310 longitudinal crack (synonymous with splaying) and showed that the creation of debris took place by
 311 bending causing intralaminar cracks (Fig. 22). Therefore the dynamic and static failure mode was
 312 fragmentation, with smaller debris in dynamics, which dissipated more energy.

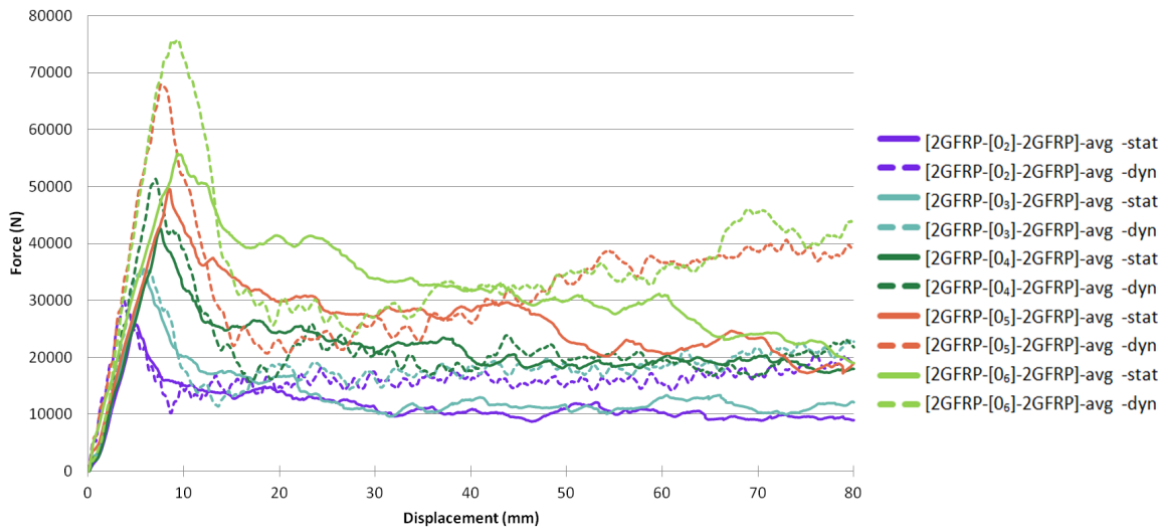


313
314

Fig. 21: Comparison of static and dynamic failure patterns of [GFRP] tubes via microscopic observation.

315

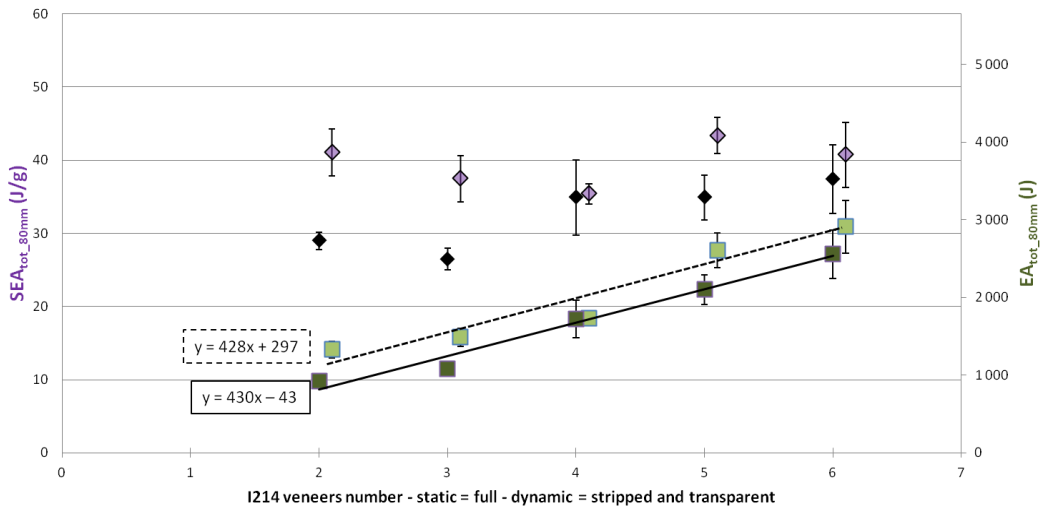
316 Now, the results for the sandwich tubes are discussed. The averaged curves of static and dynamic test
 317 results versus the number of poplar layers have been superimposed in Fig. 23.



318
319

Fig. 22: Averaged dynamic and static force-displacement curves of tubes $[2GFRP-[0_n]-2GFRP]_{2 \leq n \leq 6}$

320 A first observation concerns the change of the apparent slope between static and dynamic conditions. In
 321 dynamics, the slope is greater than in static (Fig. 23) for all configurations. As the pseudo-linear slope of
 322 the glass fibre tubes also changed between the static and dynamic regimes, this behaviour can be
 323 attributed to the I214 poplar, the glass fibres or the coupling of the two materials. The second
 324 observation is that the performance of sandwich tubes with glass fibre skins was improved in dynamics
 325 (Fig.24).

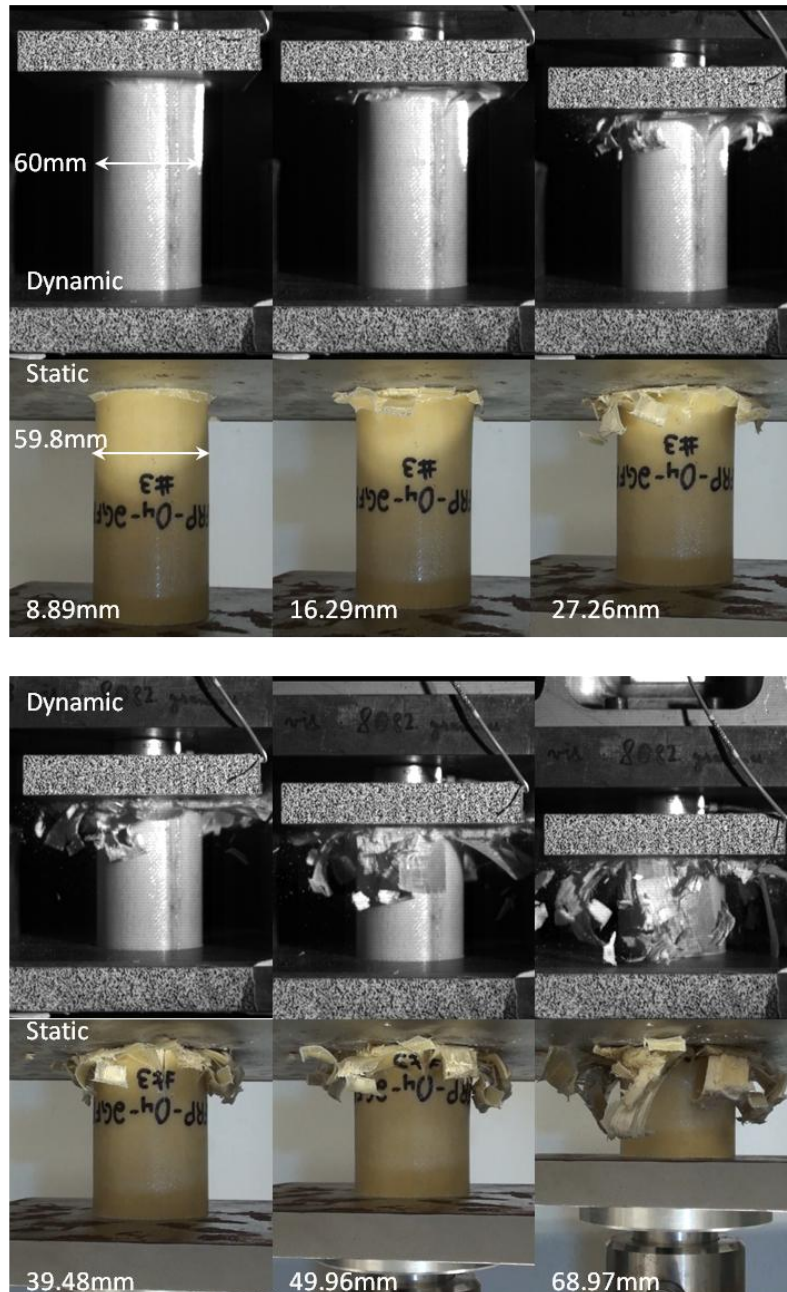


326
327
328

Fig. 24: Evolution of $EA_{tot,80mm}$ and $SEA_{tot,80mm}$ according to the number of I214 plies in static and dynamic for tubes with glass skins.

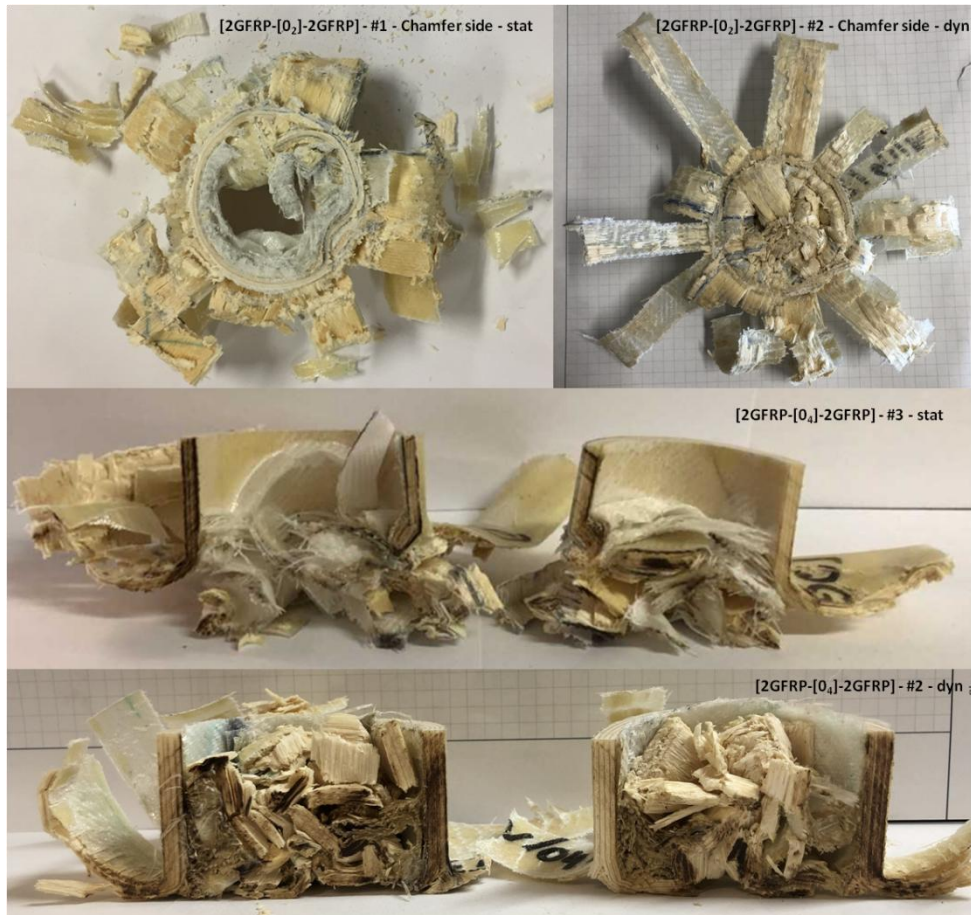
329 The slope modelling the absorbed energy presented an identical director coefficient in dynamics and
 330 statics. In addition, the average crushing stress of an I214 ply surrounded by glass fibres changed very
 331 little or not at all between the static (24.3 MPa) and the dynamic (25 MPa) tests. The comparison of

332 static and dynamic post-mortem failure patterns showed a fairly similar mode of failure with mainly the
 333 formation of petals after splaying (Fig. 25). However, the local buckling observed in statics disappeared
 334 in dynamics and the compaction of debris was much greater in dynamics than in statics, as for tubes
 335 with carbon skins (Fig. 26). The debonding of interior fibreglass skins was also much greater in static
 336 than in dynamic.



337
 338
 339

Fig. 25: Static and dynamic comparison of the failure mode of the tube [2GFRP-[0₄]-2GFRP]-#3 at iso-displacement (the static images have been turned).



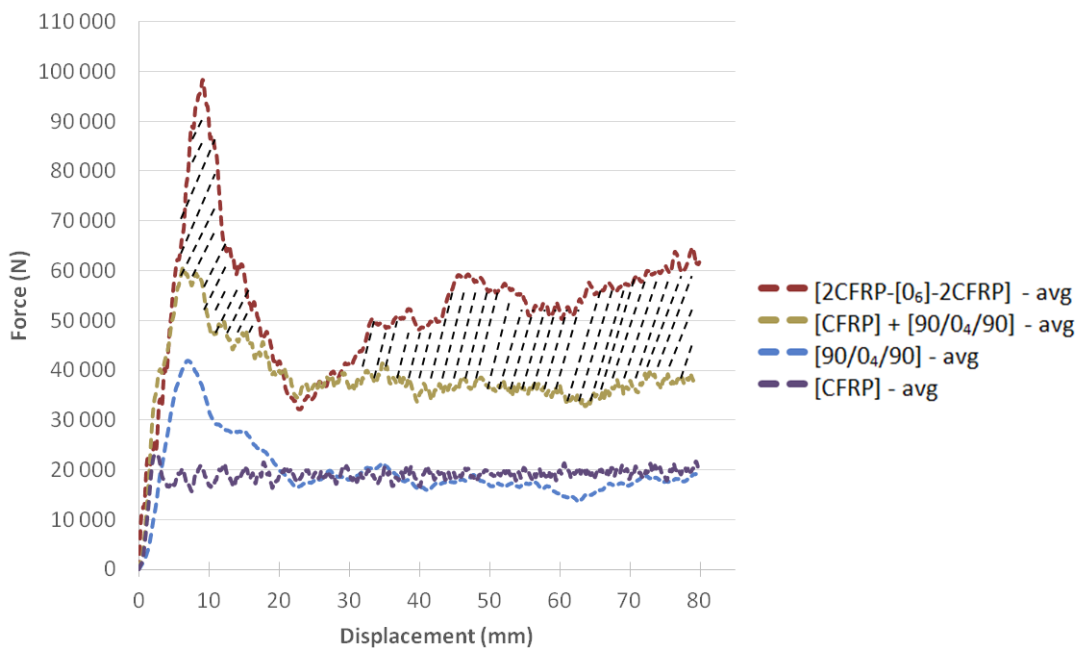
340
341 **Fig. 26: Static and dynamic comparison of the post-mortem failure pattern for tubes with glass skins.**

342
343 **3.4. Coupling gains between wood core and composite skins**

344 To assess the coupling effects, the approach adopted was as follows. The crushed tubes [CFRP] and
 345 [GFRP] shown in Tab. 4 and Tab. 5 correspond to the equivalent of the outer and inner skins of
 346 sandwich tubes [2CFRP-[0₆]-2CFRP] and [2GFRP-[0₆]-2GFRP]. For the equivalent of these sandwich
 347 tubes using wood core alone, it was not possible to consider the poplar-only tubes [0₆] (6 layers in the
 348 longitudinal direction) as, due to a very unstable mode of failure, the possible contribution of the wood to
 349 the energy absorption was very low and not significant [29]. So the most stable configuration, still with
 350 six layers of poplar but with only four plies in the longitudinal direction [90/0₄/90] was considered for the
 351 reference of the wood core. By cumulating the crushing of the tubes [CFRP] (or [GFRP]) and the
 352 equivalent of the core [90/0₄/90], and comparing them to the direct crushing of the tubes [2CFRP-[0₆]-
 353 2CFRP] (or [2GFRP-[0₆]-2GFRP]), the coupling effect was deduced.

355 **3.4.1. Tubes with Carbon skins**

356 The results are presented in Fig. 27 and Tab. 6 and the results obtained in static [30] are recalled. A
 357 gain of 41% can be noted for the strength of the plate, 35% for the energy absorbed and 40% for the
 358 SEA, showing the interest of merging these materials. However, the gain is slightly lower than in static
 359 conditions (Tab. 6). This slightly lower gain can be explained by the fact that the CFRP tube alone
 360 shows an improvement in its dynamic SEA (+ 14.6 J/g), while the sandwich tube with carbon fibre skins
 361 keeps an identical SEA (0.5 J/g difference).



362 **Fig. 27: Dynamic coupling for sandwich [2CFRP-[0₆]-2CFRP]**

363

364

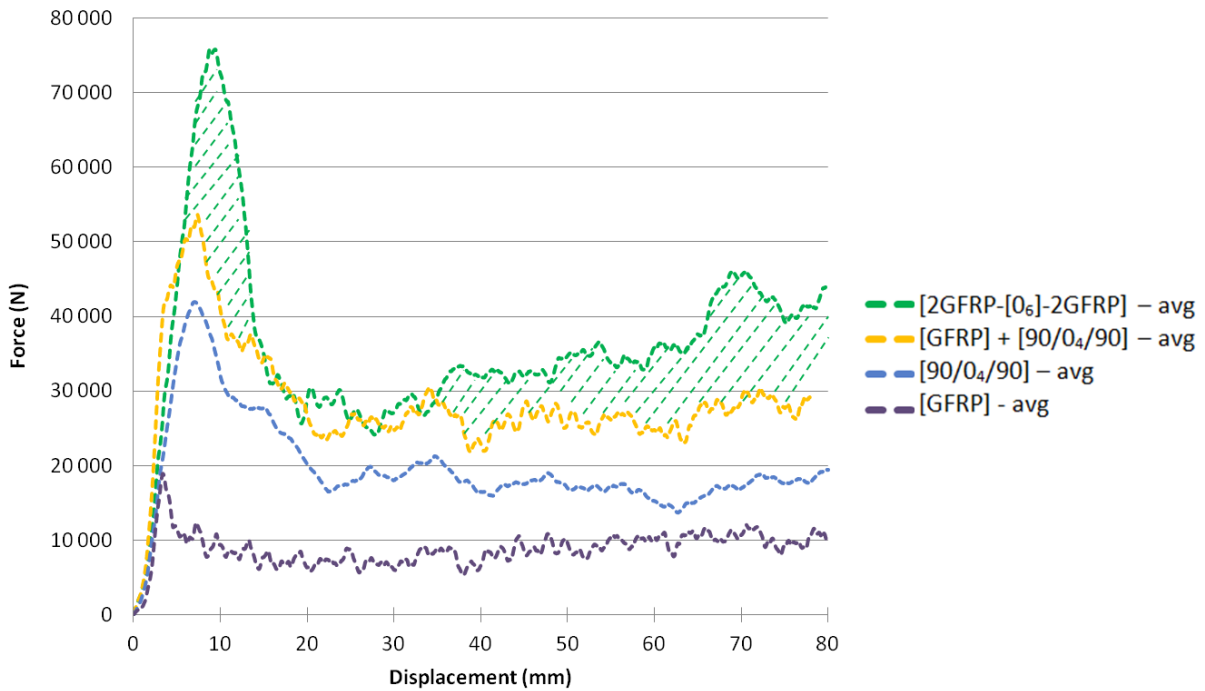
| | F_{plateau} N | EA_{tot, 80mm} J | Mass g | SEA_{tot, 80mm} J/g |
|---------|--|---|-------------------------|--|
| Static | [90/0 ₄ /90] - avg | 21 019 | 1 632 | 76.6 |
| | [CFRP] - avg | 15 570 | 1 247 | 27.7 |
| | [90/0 ₄ /90] + [CFRP] - avg | 36 589 | 2 879 | 104.3 |
| | [2CFRP-[0 ₆]-2CFRP] - avg | 55 551 | 4 264 | 102.9 |
| | Coupling gain | 52% | 48% | 47% |
| Dynamic | [90/0 ₄ /90] - avg | 17 940 | 1 618 | 72.8 |
| | [CFRP] - avg | 19 249 | 1 516 | 27.6 |
| | [90/0 ₄ /90] + [CFRP] - avg | 37 189 | 3 134 | 100.4 |
| | [2CFRP-[0 ₆]-2CFRP] - avg | 52 459 | 4 235 | 102.0 |
| | Coupling gain | 41% | 35% | 40% |

365 **Tab. 6: Gain obtained by coupling wood core and carbon skins.**

366

3.4.1. Tubes with glass skins

367 The dynamic coupling for glass skins is shown in Fig. 28 and Tab 7.



368
369

Fig. 28: Dynamic coupling for sandwich [2GFRP-[0₆]-2GFRP]

370 The dynamic coupling allowed gains of 20% and 22% on the absorbed energy and the SEA,
371 respectively (Tab. 7). The gain of the coupling in dynamics was slightly lower than that obtained in
372 statics: the [GFRP] tube showed a gain in SEA of 20.2 J / g between the static and the dynamic tests,
373 resulting in an energy difference of 330 J.

| | $F_{plateau}$ N | EA_{tot_80mm} J | Mass g | SEA_{tot_80mm} J/g | |
|---------|--|-----------------------|-----------|--------------------------|------|
| Static | [90/0 ₄ /90] - avg | 21 019 | 1 632 | 76.6 | 30.6 |
| | [GFRP] - avg | 4 670 | 364 | 24.0 | 21.4 |
| | [90/0 ₄ /90] + [GFRP] - avg | 25 689 | 1 996 | 100.6 | 29.9 |
| | [2GFRP-[0 ₆]-2GFRP] - avg | 28 995 | 2 556 | 99.2 | 37.4 |
| | Coupling gain | 13% | 28% | | 25% |
| Dynamic | [90/0 ₄ /90]-avg | 17 940 | 1 618 | 72.8 | 31.5 |
| | GFRP - avg | 8 827 | 694 | 25.0 | 41.6 |
| | [90/0 ₄ /90] + GFRP - avg | 26 767 | 2 312 | 97.8 | 31.8 |
| | [2GFRP-[0 ₆]-2GFRP] - avg | 35 851 | 2 908 | 103.7 | 40.7 |
| | | 25% | 20% | | 22% |

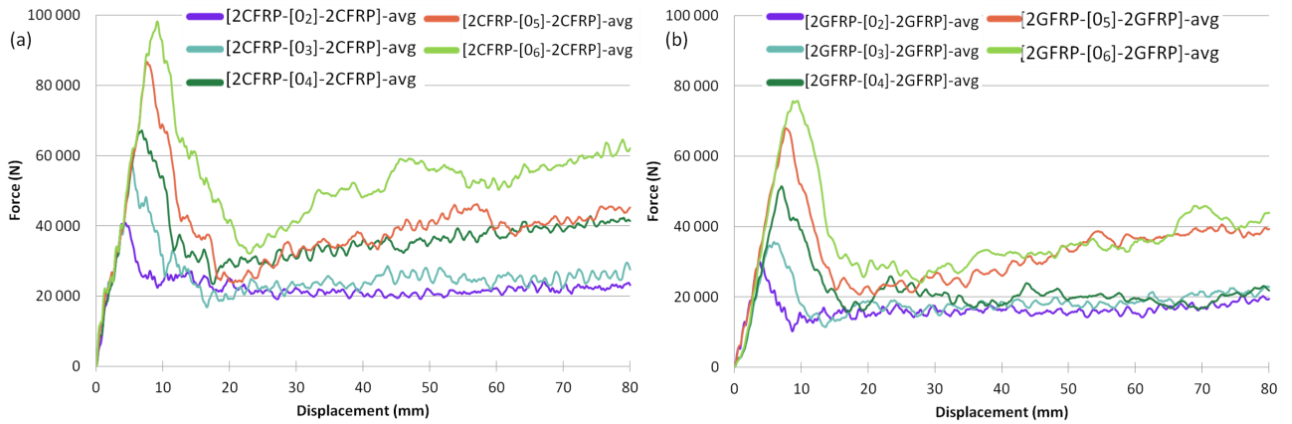
374

Tab. 7: Gain obtained by coupling wood core and glass skins.

375

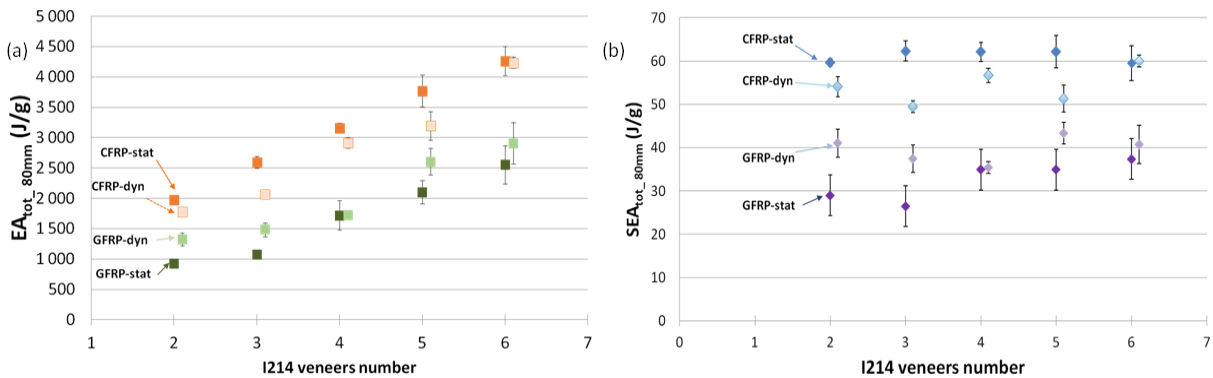
376 **3.5. Comparison of tubes with carbon and glass skins**

377 Fig. 29 shows a superposition of the dynamic curves of the glass and carbon fibre sandwich tubes.



378 **Fig. 29: Comparison of dynamic crushing of (a) CFRP and (b) GFRP skins.**

380 The peak load on tubes with carbon fibre skins is higher than for those made of glass fibres. Average
 381 stress levels on carbon fibres are higher than those obtained with glass fibres. The energies absorbed
 382 and the SEA according to the types of skin and the number of I214 layers are compared in Fig. 30.



383 **Fig. 30: Evolution of (a) EA_{tot,80mm} (b) SEA_{tot,80mm} according to the number of poplar layers, the nature of the skins,**
 384 **and static and dynamic conditions.**

386 The energy absorbed, whether with carbon fibre or glass fibre skins, has an almost linear relationship
 387 with the number of I214 poplar veneers. The linear increase in absorbed energy does not lead to an
 388 increase in SEA, which can be considered almost constant. In static and for carbon fibre skins, the SEA
 389 oscillates around a value of 61.2 J / g and, in dynamics, around an average value of 54.3 J / g. With the
 390 fibreglass skins, in static mode and with the passage from 3 to 4 plies, a slight increase in the SEA is to
 391 be noted before it stagnates at a value of 35.7 J / g. Dynamically, glass fibre skins exhibit a more regular
 392 SEA oscillation around an average value of 39.5 J / g.
 393

394

395 **4. Conclusions and perspectives**

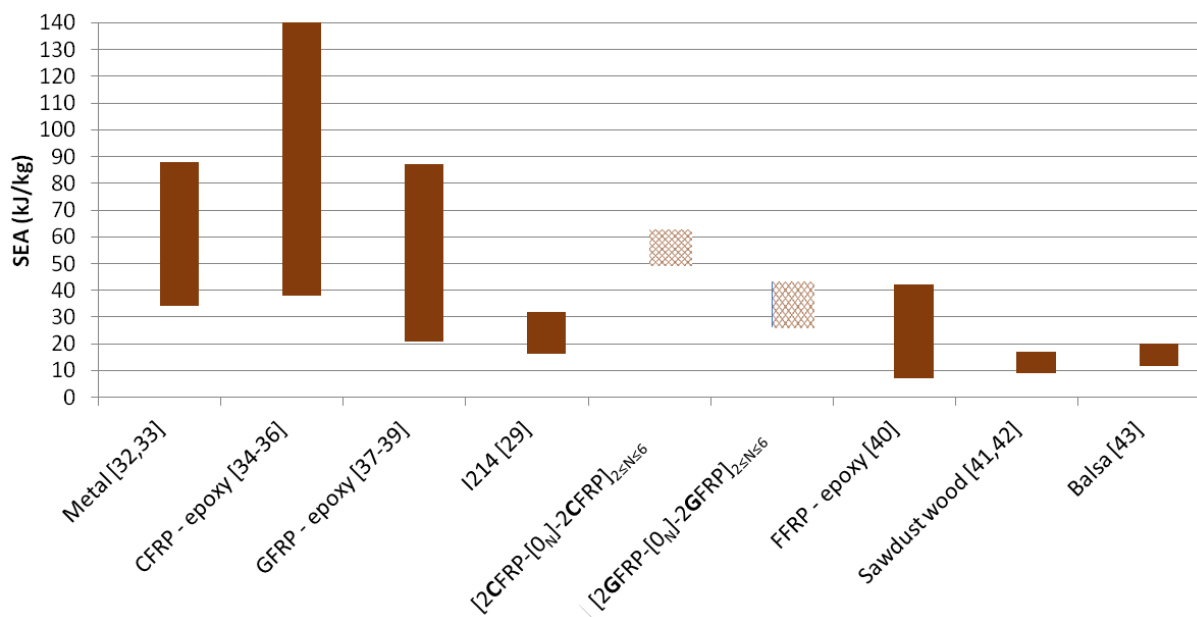
396 Dynamic crushing tests of sandwich tubes with carbon fibre or glass - epoxy resin skins and poplar
397 veneer core were investigated experimentally in this study. The tests showed that:

398 - The dynamic crushing of sandwich tubes with carbon skins [2CFRP-[0_N]-2CFRP]_{2≤N≤6} gave
399 interesting energy absorption results: an average dynamic SEA of 54.3 J / g. As the energy
400 absorbed evolved linearly with the number of I214 layers employed, the dynamic SEA oscillated
401 between 49.4 and 60 J/g. The monolithic CFRP tube had an SEA of 81.3 J/g versus a
402 maximum of 60 J/g but the plateau force was 52,459 N for the sandwiches and 19,249 N for the
403 CFRP tubes alone. An increase in the initial pseudo-linear slope between statics and dynamics
404 was also observed. This can be attributed either to the carbon or to the wood or to the coupling
405 of the two, since these two materials also showed an increase in apparent modulus in
406 dynamics. The predominant failure mode in statics and dynamics was splaying. In dynamics,
407 the internal confinement of debris was more pronounced than in statics. The combined use of
408 poplar and carbon fibres allowed a gain on the SEA of the order of 40% in dynamics compared
409 to the sum of the two materials crushed independently.

410 - The dynamic crushing of sandwich tubes with glass skins [2GFRP-[0_N]-2GFRP]_{2≤N≤6} also
411 showed interesting energy absorption results. An average SEA of 39.3 J / g was obtained in
412 dynamic tests. The static and dynamic failure patterns of these tubes showed the formation of
413 petals induced by splaying. The internal containment of debris was more marked in dynamics
414 than in statics. The crushing of a monolithic glass fibre tube (of the same thickness as the skins)
415 showed a strong improvement in its dynamic energy absorption properties: its unstable crushing
416 in static generated large pieces of debris whereas the creation of fewer large and more
417 microscopic pieces in dynamic led to more dissipative properties, raising the SEA from 21.4 J /
418 g to 41.6 J / g. With the glass fibre skins in dynamics, the insertion of the I214 veneers as core
419 materials allowed an elevation of the crush plate for an equivalent SEA and also presented

420 interesting coupling of the two materials, with a gain of 20 % of energy absorbed and 22% on
 421 SEA. In the same way as with carbon fibre skins, the transition from static to dynamic produced
 422 a greater load peak and a pseudo-linear slope.

423 Globally, the dynamic behaviour of these sandwiches with a poplar core confirms the results obtained in
 424 statics and the significant contribution in terms of energy absorbed by the wood core. Indeed, when the
 425 number of poplar layers of the core increase from two to six, the absorbed energy is doubled. The SEA
 426 obtained for the configurations studied is comparable to those of other materials (Fig. 33) but minimizes
 427 the use of composites in favour of wood. Because poplar is a wood species with a relatively low density,
 428 and thus with some of the lowest intrinsic mechanical characteristics, work on various wood species is
 429 envisaged in order to study their crash aptitudes and compare their behaviour and performance with
 430 those of poplar I214.



431
 432 Fig. 23: SEA from of some materials ([29], [30]).

433
 434 **5. Acknowledgements**

435 The authors thank the French Government for providing financial support (MESRI) and the Garnica
 436 company for providing I214 veneers for this study.

437 **6. References**

- 438 [1] Forest Product Laboratory. Wood Handbook Wood as an Engineering Material. United States
439 Department of Agriculture, Forest Service; 2010.
440
- 441 [2] R. Bergman, M. Puettmann, A. Taylor, and K.E. Skog, "The Carbon Impacts of Wood Products,"
442 *For. Prod. J.* vol. 64, pp 220–31, 2014. <https://doi.org/10.13073/FPJ-D-14-00047>.
443
- 444 [3] R. Asada, G. Cardellini, C. Mair-Bauernfeind, J. Wenger, V. Haas, D. Holzer, et al., "Effective
445 bioeconomy? A MRIO-based socioeconomic and environmental impact assessment of generic
446 sectoral innovations," *Technol. Forecast. Soc. Change.* Vol 153, n°119946,
447 2020;153:<https://doi.org/10.1016/j.techfore.2020.119946>.
448
- 449 [4] B. Castanie, C. Bouvet, M. Ginot, "Review of composite sandwich structure in aeronautic
450 applications," *Comp. Part. C Open Access*, Vol. 1, n° 100004, 2020.
451 <https://doi.org/10.1016/j.jcomc.2020.100004>.
452
- 453 [5] <https://www.robin-aircraft.com/> accessed 2021/07/09
454
- 455 [6] <https://www.avionsmauboussin.fr/> accessed 2021/07/09
456
- 457 [7] <https://aura-aero.com/> accessed 2021/07/09
458
- 459 [8] D. Kohl, P. Link and S. Böhm, "Wood as a Technical Material for Structural Vehicle Components,"
460 *Procedia CIRP*, Vol. 40, pp 557–61, 2016. <https://doi.org/10.1016/j.procir.2016.01.133>.
461
- 462 [9] Consortium WoodC.A.R. <https://www.woodcar.eu/index.html>. accessed 2021/07/09
463
- 464 [10] J. Susainathan, F. Eyma, E. De Luycker, A. Cantarel and B. Castanie, "Manufacturing and quasi-
465 static bending behavior of wood-based sandwich structures," *Comp. Struct.*, Vol. 182, pp 487–504,
466 2017. <https://doi.org/10.1016/j.compstruct.2017.09.034>.
467
- 468 [11] J. Smardzewski and K.W. Wojciechowski, "Response of wood-based sandwich beams with three-
469 dimensional lattice core," *Comp. Struct.*, Vol. 2016, pp 340–49, 2019.
470 <https://doi.org/10.1016/j.compstruct.2019.03.009>.
471
- 472 [12] S.W. Kavermann and D. Bhattacharyya, "Experimental investigation of the static behaviour of a
473 corrugated plywood sandwich core," *Comp. Struct.* Vol. 207, pp 836–44, 2019.
474 <https://doi.org/10.1016/j.compstruct.2018.09.094>.
475
- 476 [13] J. Liu , T. Zhang, W. Jiang Wand J. Liu, "Mechanical response of a novel composite Y-frame core
477 sandwich panel under shear loading" *Comp. Struct.*, Vol. 224, n° 111064, 2019.
478 <https://doi.org/10.1016/j.compstruct.2019.111064>.
479
- 480 [14] J. Smardzewski, "Experimental and numerical analysis of wooden sandwich panels with an auxetic
481 core and oval cells," *Mat. Des.*, Vol. 183, n° 108159, 2019.
482 <https://doi.org/10.1016/j.matdes.2019.108159>.
483
- 484 [15] X. Wang, X. Shi, Q. Meng, Y. Hu and L. Wang, "Bending behaviors of three grid sandwich
485 structures with wood facing and jute fabrics/epoxy composites cores," *Comp. Struct.*, Vol. 252,
486 n°112666, 2020. <https://doi.org/10.1016/j.compstruct.2020.112666>.
487

- 488 [16] F. Neveu, B. Castanié and P. Olivier, "The GAP methodology: a new way to design composite
489 structures," *Materials & Design*, Vol. 172, n° 107755, 2019.
490 <https://doi.org/10.1016/j.matdes.2019.107755>
491
- 492 [17] C. Atas and C. Sevim, "On the impact response of sandwich composites with cores of balsa wood
493 and PVC foam," *Comp. Struct.*, Vol.93, pp 40–48, 2010.
494 <https://doi.org/10.1016/j.compstruct.2010.06.018>.
495
- 496 [18] J. Susainathan, F. Eyma, E. De Luycker, A. Cantarel and B Castanié," Experimental investigation of
497 impact behavior of wood-based sandwich structures," *Comp. Part A, Appl. Sci. Manuf.*, Vol. 109, pp
498 10-19, 2018. . <https://doi.org/10.1016/j.compositesa.2018.02.029>.
499
- 500 [19] J. Susainathan, F. Eyma, E. De Luycker, A. Cantarel and B Castanié," Numerical modeling of
501 impact on wood-based sandwich structures", *Mech. Adv. Mat. Struct.*, Vol. 27, pp 1583–98, 2020.
502 <https://doi.org/10.1080/15376494.2018.1519619>.
503
- 504 [20] T.K. Demircioğlu, F. Balıkoğlu, O. İnal, N. Arslan, I. Ay and A. Ataş, " Experimental investigation on
505 low-velocity impact response of wood skinned sandwich composites with different core configurations,"
506 *Mat. Today. Com.*, Vol. 17, pp 31–9, 2018. <https://doi.org/10.1016/j.mtcomm.2018.08.003>.
507
- 508 [21] J. Smardzewski, Wooden sandwich panels with prismatic core – Energy absorbing capabilities.
509 *Comp. Struct.*, Vol. 230, n° 111535, 2019. <https://doi.org/10.1016/j.compstruct.2019.111535>.
510
- 511 [22] G. Palomba, G. Epasto and V. Crupi, "Lightweight sandwich structures for marine applications: a
512 review", *Mechanics of Advanced Materials and Structures*, on line,
513 <https://doi.org/10.1080/15376494.2021.1941448>
514
- 515 [23] W. Johnson, "Historical and present-day references concerning impact on wood," *Int. J. Impact*.
516 *Eng.*, Vol. 4, pp 161–74, 1986. [https://doi.org/10.1016/0734-743X\(86\)90003-5](https://doi.org/10.1016/0734-743X(86)90003-5).
517
- 518 [24] J. Susainathan, F. Eyma, E. De Luycker, A. Cantarel, C. Bouvet and B Castanié, "Experimental
519 investigation of compression and compression after impact of wood-based sandwich structures", *Comp*.
520 *Struct.*, Vol. 220, pp 236–49, 2019. <https://doi.org/10.1016/j.compstruct.2019.03.095>.
521
- 522 [25] B. Castanié, J. J. Barrau, J. P. Jaouen, and S. Rivallant, "Combined shear/compression structural
523 testing of asymmetric sandwich structures," *Exp. Mech.*, vol. 44, no. 5, pp. 461–472, 2004.
524 DOI:10.1007/BF02427957.
525
- 526 [26] F. Balıkoğlu T.K. Demircioğlu, O. İnal, N. Arslan and A. Ataş, "Compression after low velocity
527 impact tests of marine sandwich composites: Effect of intermediate wooden layers," *Comp. Struct.*,
528 Vol. 183, pp 636–42, 2018. <https://doi.org/10.1016/j.compstruct.2017.08.003>.
529
- 530 [27] M. Neumann. Investigation of the Behaviour of Shock-Absorbing Structural Parts of Transport
531 Casks Holding Radioactive Substances in Terms of Design Testing and Risk Analysis. Bergische
532 Universität Wuppertal, 2009.
533
- 534 [28] N. Butler, "Computer modelling of wood-filled impact limiters" *Nucl. Eng. Des.*, Vol. 150, pp 417–
535 24,1994. [https://doi.org/10.1016/0029-5493\(94\)90161-9](https://doi.org/10.1016/0029-5493(94)90161-9).
536

- 537 [29] R. Guélou, F. Eyma, A. Cantarel, S. Rivallant, B. Castanié, "Crashworthiness of poplar wood
538 veneer tubes", *Int. J. Impact. Eng.*, Vol. 147, n° 103738, 2021.
539 <https://doi.org/10.1016/j.ijimpeng.2020.103738>.
540
- 541 [30] R. Guélou, F. Eyma, A. Cantarel, S. Rivallant, B. Castanié, "Static crushing of wood based
542 sandwich composite tubes," *Comp. Struct.*, Vol. 273, n° 114317, 2021.
543 <https://doi.org/10.1016/j.compstruct.2021.114317>.
544
- 545 [31] D. Guillon, « Etude des mécanismes d'absorption d'énergie lors de l'écrasement progressif de
546 structures composites à base de fibre de carbone », PhD Thesis. Institut Supérieur de l'Aéronautique et
547 de l'Espace, ISAE, Ecole doctorale : Mécanique, énergétique, génie civil et procédés, 2008.
548
549